

Ginsburg-Landau theory of solid and supersolid and their possible applications to 4He

Jinwu Ye

Department of Physics, The Pennsylvania State University, University Park, PA, 16802

(Dated: December 2, 2024)

We construct a Ginsburg Landau (GL) theory to map out the 4He phase diagram, analyze carefully the conditions for the existence of the supersolid (SS) and study all the phases and phase transitions in a unified framework. In this GL, we put the two competing orders between the solid component and the superfluid component on the same footing. We only introduce two parameters: v is the repulsive interaction between the normal component and the local superfluid mode and g is a periodic changing chemical potential for the local superfluid mode. The microscopic origins of v and g are given. By using this GL action, we study the superfluid to supersolid transition, normal solid to the supersolid transition and analyze the conditions for the existence of the supersolid. The NCRI in the SS state is calculated and found to be isotropic in *bcc* and *fcc* lattice, but weakly anisotropic in *hcp* lattice. We study the elementary low energy excitation inside a supersolid. We find that there are two longitudinal "supersolidon" modes (one upper branch and one lower branch) inside the SS, while the transverse modes in the SS stay the same as those inside the NS. Detecting the two supersolidon modes by various equilibrium and thermodynamic experiments such as X-ray scattering, neutron scattering, acoustic wave attenuation and heat capacity can prove or disapprove the existence of a supersolid in Helium 4. We also work out the experimental signatures of these elementary excitations in Debye-Waller factor, density-density correlation, vortex loop interaction and specific heat. The estimated excess entropy due to vacancies seems consistent with data measured in the specific experiment. We also make comments on torsional oscillator experiments and other related experiments. A toy model of supersolid wavefunction is analyzed. The difference and similarities with lattice supersolid are clearly demonstrated.

I. INTRODUCTION

A solid can not flow. It breaks a continuous translational symmetry into a discrete lattice translational symmetry. There are low energy lattice phonon excitations in the solid. While a superfluid can flow even through narrowest channels without any resistance. It breaks a global $U(1)$ phase rotational symmetry and has the off-diagonal long range order (ODLRO)¹. There are low energy superfluid phonon excitations in the superfluid. A supersolid is a state which breaks both the continuous translational symmetry and the global $U(1)$ symmetry, therefore has both the crystalline order and the ODLRO. The possibility of a supersolid phase in 4He was theoretically speculated in 1970^{2,3,4,5}. Andreev and Lifshitz proposed the Bose-Einstein condensation of vacancies as the mechanism of the formation of supersolid². Chester wrote down a wavefunction which has both ODLRO and crystalline order and also speculated that a supersolid cannot exist without vacancies or interstitial³. Leggett proposed that solid 4He might display Non-Classical Rotational Inertial (NCRI) which is a low temperature reduction in the rotational moment of inertia due to the superfluid component of solid 4He ^{4,5,6}. Leggett also suggested that quantum tunneling of He atoms between neighboring sites in a crystal can also lead to a supersolid even in the absence of vacancies. Over the last 35 years, a number of experiments have been designed to search for the supersolid state without success. However, recently, by using torsional oscillator measurement, a PSU group lead by Chan observed a marked $1 \sim 2\%$ NCRI of solid 4He at $\sim 0.2K$, both when embedded in Vycor glass⁷ and in bulk 4He ⁸. Some of the important experimental facts are: (1) the

NCRI slides towards the normal solid regime with a very long tail. (2) the superfluid fraction has a non-monotonic dependence on the pressure, it increases first, reaches a maximum at ~ 55 bar, then decreases to zero at a much higher pressure $p_{c2} \sim 170$ bar¹⁰. (3) the supersolid has a very low critical velocity corresponding to $\sim 1 - 3$ flux quanta above which the NCRI is reduced (4) a very tiny fraction of $He3$ in the range of $x \sim 40ppB - 85ppM$ decreases the superfluid fractions, but increases the supersolid to normal solid transition temperature considerably. This observation is very counter-intuitive and in sharp contrast to the effects of $He3$ impurities in both 3d 4He superfluid and 2d superfluid 4He films. (5) Although the previous specific heat measurement at 3He impurities concentration $x \sim 30$ ppM to temperature as low as $100mK$ did not detect any obvious specific heat anomaly⁹, very recent much more refined specific heat measurements in the range $x \sim 0.3 - 3$ ppM to temperature as low as 45 mK found a broad excessive specific heat (after subtracting the Debye term) peak around the putative supersolid onset critical temperature ~ 100 mK. The authors suggested that the supersolid state of 4He maybe responsible for the NCRI. They mapped out the experimental global phase diagram of 4He in the Fig.4 in⁸. More recently, the PSU group detected about 10^{-4} reduction in the rotational inertial in solid H_2 ¹¹, but by performing blocked cell experiments, the authors concluded that the reduction is *classical* due to the motion of *HD* impurities clustering. So the PSU group did not find any NCRI in solid hydrogen¹¹.

The PSU experiments inspired us to reexamine the already fantastic physics in 4He and rekindled extensive both theoretical^{12,13,14,15} and experimental^{18,19,20}

interests in the still controversial supersolid phase of 4He . There are two kinds of complementary theoretical approaches. The first is the microscopic numerical simulation¹². The second is the phenomenological approach^{13,14,15,16}. At this moment, despite all the theoretical work, there is no consensus yet on the interpretation of PSU's experiments. Torsional oscillator measurement is essentially a dynamic measurement, as suggested in¹², several possibilities can lead to the NCRI observed in the Kim-Chan experiments, although the supersolid state is the most interesting case, it is just one of these possibilities. Obviously, many other thermodynamic and equilibrium measurements are needed to make a definite conclusion. A solid has the order in the number density, while a superfluid has the order in the phase. The two phases are in totally different extremes of the state of matter. How to combine the two opposite extremes into a new state of matter, supersolid, is an important and interesting topic on its own. It is widely believed that the only chance to get a supersolid is that the solid is not *perfect*, namely, it is an incommensurate solid which has defects such as vacancies or interstitials, so the total number of bosons can fluctuate to give some rooms for the invasion of superfluid. Due to large zero point motions, there are indeed rapid exchanging between local 4He atoms in bulk 4He , but this local process will not lead to a global phase ordering. It was estimated from both X-ray scattering experiments²⁹ and some microscopic calculations¹² that the thermal excitation energies of a vacancy and interstitial are $\epsilon_v \sim 10 K$, $\epsilon_i \sim 40 K$, so thermal fluctuations favor vacancies over interstitials. Because both have very high energy, so the thermal generated vacancies and interstitials are irrelevant around $45 \sim 200 mK$. However, it is still possible that there are quantum fluctuation generated vacancies and interstitials even at $T = 0$. It is still not known if quantum fluctuations favor vacancies over interstitials or not¹⁵.

In this paper, we will construct a phenomenological Ginsburg Landau (GL) theory to study all the possible phases and phase transitions in helium 4 system. We identify order parameters, symmetry and symmetry breaking patterns in all the phases. Particularly, we will address the following two questions: (1) What is the condition for the existence of the SS state ? (2) If the SS exists, what are the properties of the supersolid to be tested by possible new experiments. Let's start by reviewing all the known phases in 4He . The density of a normal solid (NS) is defined as $n(\vec{x}) = n_0 + \sum'_{\vec{G}} n_{\vec{G}} e^{i\vec{G} \cdot \vec{x}} = n_0 + \delta n(\vec{x})$ where $n_{\vec{G}}^* = n_{-\vec{G}}$ and \vec{G} is any non-zero reciprocal lattice vector. In a normal liquid (NL), if the static liquid structure factor $S(k)$ has its first maximum peak at \vec{k}_n , then near k_n , $S(k) \sim \frac{1}{r_n + c(k^2 - k_n^2)^2}$. If the liquid-solid transition is weakly first order, it is known that the classical

free energy to describe the NL-NS transition is²⁵:

$$f_n = \sum_{\vec{G}} \frac{1}{2} r_{\vec{G}} |n_{\vec{G}}|^2 - w \sum_{\vec{G}_1, \vec{G}_2, \vec{G}_3} n_{\vec{G}_1} n_{\vec{G}_2} n_{\vec{G}_3} \delta_{\vec{G}_1 + \vec{G}_2 + \vec{G}_3, 0} + u_n \sum_{\vec{G}_1, \vec{G}_2, \vec{G}_3, \vec{G}_4} n_{\vec{G}_1} n_{\vec{G}_2} n_{\vec{G}_3} n_{\vec{G}_4} \delta_{\vec{G}_1 + \vec{G}_2 + \vec{G}_3 + \vec{G}_4, 0} + (1)$$

where $r_{\vec{G}} = r_n + c(G^2 - k_0^2)^2$ is the tuning parameter controlled by the pressure or temperature. Note that the average density n_0 does not enter in the free energy. Because the instability happens at finite wavevector, Eqn.1 is an expansion in terms of small parameter $n_{\vec{G}}$ alone, it is *not a gradient expansion* ! The GL parameters w and u_n may be determined by fitting the theoretical predictions with experimental data. It is easy to see that Eqn.1 is invariant under $\vec{x} \rightarrow \vec{x} + \vec{a}$, $n(\vec{x}) \rightarrow n(\vec{x} + \vec{a})$, $n(\vec{G}) \rightarrow n(\vec{G}) e^{i\vec{G} \cdot \vec{a}}$ where \vec{a} is any vector. In the NL, $\langle n(\vec{G}) \rangle = 0$, the translational symmetry is respected. In the NS, $\langle n(\vec{G}) \rangle \neq 0$, the symmetry is broken down to translational invariance under only a lattice constant $\vec{a} = \vec{R}$, $\vec{G} \cdot \vec{R} = 2\pi n$, $n(\vec{x}) \rightarrow n(\vec{x} + \vec{R})$, $n(\vec{G}) \rightarrow n(\vec{G})$. As shown in the Fig.1, the NL to NS transition only happens at finite temperature, so the classical theory is valid. Note that due to the lack of the Z_2 symmetry of $\delta n(\vec{x}) \rightarrow -\delta n(\vec{x})$, namely, $n_{\vec{G}} \rightarrow -n_{\vec{G}}$, there is always a cubic w term which makes the the NL to NS a 1st order transition. The u_n term which is invariant under the Z_2 symmetry is needed for the stability reason.

Of course, the Superfluid to Normal Liquid transition at finite temperature in the Fig.1 is the 3d XY transition described by²⁴:

$$f_{\psi} = K |\nabla \psi|^2 + t |\psi|^2 + u |\psi|^4 + \dots \quad (2)$$

where ψ is the complex order parameter and t is the tuning parameter controlled by the temperature or pressure. Eqn.2 is invariant under the global $U(1)$ symmetry $\psi \rightarrow \psi e^{i\theta}$. In the NL, $\langle \psi \rangle = 0$, the symmetry is respected. In the SF, $\langle \psi \rangle \neq 0$, the symmetry is broken. The GL parameters K, t, u may be determined by fitting the theoretical predictions with experimental data.

The coupling between $n(\vec{x})$ and $\psi(\vec{x})$ consistent with all the symmetry can be written down as:

$$f_{int} = g \delta n(\vec{x}) |\psi(\vec{x})|^2 + v (\delta n(\vec{x}))^2 |\psi(\vec{x})|^2 + \dots \quad (3)$$

where $\delta n(\vec{x}) = n(\vec{x}) - n_0 = \sum'_{\vec{G}} n_{\vec{G}} e^{i\vec{G} \cdot \vec{x}}$. Note that the average density n_0 does not enter in the interaction either. Eqn.3 is an expansion in terms of two small parameters $\delta n(\vec{x})$ and $\psi(\vec{x})$. The \dots include the other terms in higher odd and even powers of $\delta n(\vec{x})$ which are sub-leading to the g and v term. In an effective GL theory, $n(\vec{x})$ and $\psi(\vec{x})$ emerge as two independent order parameters.

Eqn.3 is invariant under both the translational symmetry $\vec{x} \rightarrow \vec{x} + \vec{a}$, $n(\vec{x}) \rightarrow n(\vec{x} + \vec{a})$, $\psi(\vec{x}) \rightarrow \psi(\vec{x} + \vec{a})$ and the global $U(1)$ symmetry $\psi \rightarrow \psi e^{i\theta}$. Note that it

is important to keep both g and v term in the Eqn.3, because the g term changes the sign, while the v term is invariant under the Particle-Hole (PH) transformation $\delta n(\vec{x}) \rightarrow -\delta n(\vec{x})$, so the sign of g makes a difference ! Due to the two competing orders between the density fluctuation represented by $(\delta n(\vec{x}))^2$ and the local superfluid mode represented by $|\psi|^2$, we expect v to be always positive and is an increasing function of the pressure p . The positive v term is also needed for the stability reason. On the other hand, we can view g as a *periodic* chemical potential with *average zero* acting on ψ . It is easy to see the coupling is attractive $g_v < 0$ for vacancies, but repulsive $g_i > 0$ for interstitials. From Eqn.3, we can classify three kinds of solids: If $g = 0$, the C-NS has the P-H symmetry, let's call this kind of PH symmetric C-NS as NS-PH. In general, $g \neq 0$, so there is no particle-hole symmetry in the C-NS, there are still two kinds: (1) vacancy like C-NS where the excitation energy of a vacancy is lower than that of an interstitial, named NS-v. (2) interstitial like C-NS where the excitation energy of an interstitial is lower than that of a vacancy, named NS-i. We expect that in contrast to v , g is an intrinsic parameter of solid Helium 4 which depends on the mass of a 4He atom and the potential between the 4He atoms, but not sensitive to the pressure p . In SS-v and SS-i, $\psi(\vec{x})$ stands for vacancies and interstitials respectively. The total density of the system is $n_t(x) = n(x) \pm |\psi(x)|^2$ for SS-i and SS-v respectively where $n(x)$ is the density of number of sites and $|\psi(x)|^2$ is the superfluid density.

The GL equations 1,2,3 are invariant under both the translational symmetry $\vec{x} \rightarrow \vec{x} + \vec{a}$, $n(\vec{x}) \rightarrow n(\vec{x} + \vec{a})$, $n(\vec{G}) \rightarrow n(\vec{G})e^{i\vec{G} \cdot \vec{a}}$, $\psi(\vec{x}) \rightarrow \psi(\vec{x} + \vec{a})$ and the global $U(1)$ symmetry $\psi \rightarrow \psi e^{i\theta}$. In a NL, $n_{\vec{G}} = 0$, $\langle \psi \rangle = 0$. In a SF, $n_{\vec{G}} = 0$, $\langle \psi \rangle \neq 0$. In a NS, $n_{\vec{G}} \neq 0$, $\langle \psi \rangle = 0$. While in a supersolid, $n_{\vec{G}} \neq 0$, $\langle \psi \rangle \neq 0$. From the normal liquid (NL) side, one can approach both the solid and the superfluid. Inside the NL, $t > 0$, ψ has a gap, so can be integrated out from Eqn.3, we recover the solid-liquid transition tuned by $r_{\vec{G}}$ in Eqn.1 (Fig.2). Inside the NL $\langle n(\vec{x}) \rangle = n_0$, the density fluctuations of $\delta n(x)$ is massive, so can be integrated out from Eqn.3, then we recover the NL to SF transition tuned by t in Eqn.2 (Fig.1).

Quantum fluctuations can be incorporated by (1) $n(\vec{x}) \rightarrow n(\vec{x}, \tau)$ and including $\frac{1}{2}\rho_n(\partial_{\tau}n)^2$ in Eqn.1. (2) $\psi(\vec{x}) \rightarrow \psi(\vec{x}, \tau)$ and including $\psi^{\dagger}(\vec{x}, \tau)\partial_{\tau}\psi(\vec{x}, \tau)$ in Eqn.2. (3) Due to the lack of particle-hole symmetry in the normal solid, including additional terms like $\delta n(\vec{x}, \tau)\psi^{\dagger}(\vec{x}, \tau)\partial_{\tau}\psi(\vec{x}, \tau)$ in Eqn. 3. We will explicitly consider the quantum fluctuations in sections II and III where we will discuss superfluid density wave formation in ψ sector only and in section IV where we will discuss the quantum phase transition from the superfluid to the C-NS (either NS-v or NS-i). At mean field level inside a given phase, all the τ derivative terms can be neglected. In all the classical phase transitions addressed in this paper, we will also neglect these quantum fluctuation terms. However, as shown in this paper, the quantum fluctuation terms are very important in the zero temperature

quantum phase transition from SS-v (SS-i) to NS-v (NS-i) driven by the pressure (see Fig.2) and to determine the low energy excitation spectra in a given phase.

The rest of the paper is organized as the following: In sec. II, for the first time, we construct a quantum Ginsburg-Landau action to study SF to the NS transition and also explicitly establish the Feynman relation from the QGL. In Sec.III, taking into account the couplings between the n and ψ sector encoded in Eqn.3, we study the superfluid to supersolid transition which is a simultaneous combination of the SFDW transition in ψ sector driven by the roton condensation at $k_0 = k_r$ and the NS transition in the n sector driven by the divergence of the structure function at $k_0 = k_r = k_n$ discussed in Sec.II. We also sketch the global phase diagrams to be confirmed and analyzed in the following sections. In Sec.IV, we approach the SS phase from the NS side and discuss the SFDW in SS-v and SS-i respectively. We analyze carefully the conditions for the existence of SS-v. We explicitly show that the SS-v is the possible ground state when the g_v is sufficiently negative (Fig.3). The SS-i is less likely, but we still analyze SS-i in the same footing as SS-v. We also classify several common SS-i lattice structures. In sec. V, by renormalization group analysis, we study the universality class of zero temperature quantum phase transition from normal solid (NS) to supersolid (SS) driven by the pressure. In Sec.VI, we work out the non-topological elementary excitations inside the supersolids in both the isotropic solid case and the hcp lattice structure case. Then in Sec.VII, we study topological elementary excitations, namely, vortex loops and vortex lines in the SS by performing a duality transformation to the vortex loop representation. We also estimate the very large vortex core size and low critical velocity in the SS state. Then in the following sections, we study the experimental signatures of these low energy elementary excitations: In Sec. VIII, we make key predictions on the elastic X-ray scattering amplitudes from all SS-v and SS-i structures classified in Sec. IV by calculating the Debye-Waller factor and the density-density correlation function. These predictions are amenable to ongoing X-ray scattering experiments at PSU. In Sec. IX, we calculate the NCRI's in both the SF and SS states and find the NCRI in the hcp SS lattice may be weakly anisotropic. In Sec. X, we study the specific heat in the SS. In Sec. XI, we apply our theory to analyze the PSU's experiments in 4He , especially the dramatic effects of He3 impurities and also comment on several other experiments. The applications of the GL theory on Hydrogen and fermionic systems such as bilayer quantum Hall systems and electron-hole bilayer systems are also briefly mentioned. Analogy with Type-I and Type-II superconductors are made. Conclusions are summarized in the final section XII. In the appendix A, we discuss the properties of a tight-binding *toy* SS-v wavefunction. In the appendix B, we compare the properties of the SS with those of SS on extended boson Hubbard model in a lattice. Two short reports of these results appeared

in^{16,17}.

II. SUPERFLUID TO NORMAL SOLID TRANSITION

Let us start with the SF to the NS transition. In the superfluid state, if the multi-quasiparticle part can be neglected in the dynamic structure factor, the Feynman relation between the Landau quasi-particle dispersion relation in the ψ sector and the equal time structure factor in the n sector holds:

$$\omega(q) = \frac{q^2}{2mS(q)} \quad (4)$$

In the $q \rightarrow 0$ limit, $S(q) \sim q$, $\omega(q) \sim q$ recovers the superfluid phonon spectrum near $q = 0$ in the ψ_1 sector. The first maximum peak in $S(q)$ corresponds to the roton minimum in $\omega(q)$ in the ψ_2 sector (Fig.1b), namely, $k_n = k_r$. As one increases the pressure p , the interaction u also gets bigger and bigger, the first maximum peak of $S(q)$ increases, the roton minimum Δ_r gets smaller and smaller²². Across the critical pressure $p = p_c$, there are the two possibilities. (1) The resulting solid is a commensurate solid, then $\langle \psi \rangle = 0$. In the NS, there is no remnant of the roton inside the SF, the supersolid phase does not exist as an equilibrium ground state. This is the SF to the C-NS transition. In section VI, this happens when $|g|$ is sufficiently small (Fig.1). (2) The resulting solid at high pressure is an incommensurate solid with zero point quantum fluctuations generated vacancies or interstitials whose condensation leads to the formation of the SS-v and SS-i respectively. In section VI, this happens when $|g|$ is sufficiently large (Fig.2). We will discuss case (1) in this section, then the most interesting case (2) in the next section.

The effective action inside the SF is :

$$\mathcal{L}[\delta n, \theta] = i\delta n \partial_\tau \theta + \frac{1}{2}\rho_s(\nabla \theta)^2 + \frac{1}{2}\delta n V_n(\vec{q})\delta n \quad (5)$$

where ρ_s is the superfluid density and $V_n(q) = a - bq^2 + cq^4$ with $a > 0, b > 0$ is the density-density interaction between the ${}^4\text{He}$ atoms.

In the SF state, it is convenient to integrate out δn in favor of the phase field θ to get the phase representation

$$\mathcal{L}[\theta] = \frac{1}{2V_n(\vec{q})}(\partial_\tau \theta)^2 + \frac{1}{2}\rho_s(\nabla \theta)^2 \quad (6)$$

where the dispersion relation of the superfluid modes including higher orders of momentum can be extracted²⁸:

$$\omega^2 = [\rho_s V_n(\vec{q})]q^2 = 2\rho_s q^2(a - bq^2 + cq^4) \quad (7)$$

It is easy to see that the dispersion relation indeed has the form shown in Fig.1b with a roton minimum. Because the original instability comes from the density-density interaction $V_n(\vec{q})$, it is convenient to integrate

out the phase field in favor of the density fluctuation operator δn . Neglecting the vortex excitations in θ and integrating out the θ in Eqn.5 leads to:

$$\mathcal{L}[\delta n] = \frac{1}{2}\delta n(-\vec{q}, -\omega_n)[\frac{\omega_n^2}{\rho_s q^2} + V_n(\vec{q})]\delta n(\vec{q}, \omega_n) \quad (8)$$

where we can identify the dynamic pseudo-spin density-density correlation function $S_n(\vec{q}, \omega_n) = \langle \delta n(-\vec{q}, -\omega_n)\delta n(\vec{q}, \omega_n) \rangle = \frac{\rho_s q^2}{\omega_n^2 + v^2(q)q^2}$ where $v^2(q) = \rho_s V_n(q)$ is the spin wave velocity.

From the pole of the dynamic density-density correlation function, we can identify the speed of sound wave which is exactly the same as the spin wave velocity. This should be expected. From the analytical continuation $i\omega_n \rightarrow \omega + i\delta$, we can identify the dynamic structure factor: $S_n(\vec{q}, \omega) = S_n(q)\delta(\omega - v(q)q)$ where $S_n(q) = \rho_s q \pi / 2v(q)$ is the equal time density correlation function shown in Fig.1b. As $q \rightarrow 0$, $S_n(q) \rightarrow q$. The Feynman relation which relates the dispersion relation to the equal time structure factor is:

$$\omega(q) = \frac{\rho_s \pi q^2}{2S_n(q)} \quad (9)$$

which takes exactly the same form as Eqn.4 if we identify $\rho_s \sim 1/m$ with m the mass of ${}^4\text{He}$ mass. Therefore, we recovered the Feynman relation from our GL theory Eqn.5 which gives us the confidence that Eqn.5 is the correct starting action to study the the SF to SS transition. The density representation Eqn.8 is *dual* to the phase representation Eqn.6. However, the phase representation Eqn.6 contains explicitly the superfluid order parameter $\psi \sim e^{i\theta}$ which can be used to characterize the superfluid order in the SF phase. While in Eqn.8, the signature of the superfluid phonon mode is encoded in the density sound mode, because the order parameter ψ is integrated out, the superfluid order is hidden, so it is not as powerful as the phase representation in describing the SF state. However, as shown in the following, when describing the transition from the ES to the NS, the density representation Eqn.8 has a big advantage over the phase representation.

Because the instability is happening at $q = q_0$ instead of at $q = 0$, the vortex excitations in θ remain *uncritical* through the SF to SS transition. Integrating them out will generate interactions among the density δn :

$$\begin{aligned} \mathcal{L}[\delta n] = & \frac{1}{2}\delta n(-\vec{q}, -\omega_n)[\frac{\omega_n^2}{\rho_s q^2} + V_n(\vec{q})]\delta n(\vec{q}, \omega_n) \\ & - w(\delta n)^3 + u(\delta n)^4 + \dots \end{aligned} \quad (10)$$

where the momentum and frequency conservation in the quartic term is assumed. Note that the $(\omega_n/q)^2$ term in the first term stands for the quantum fluctuations of δn which is absent in the classical NL to NS transition Eqn.1. Because of the lack of Z_2 exchange symmetry, there is a cubic term in Eqn.11. Expanding $V_n(q)$ near

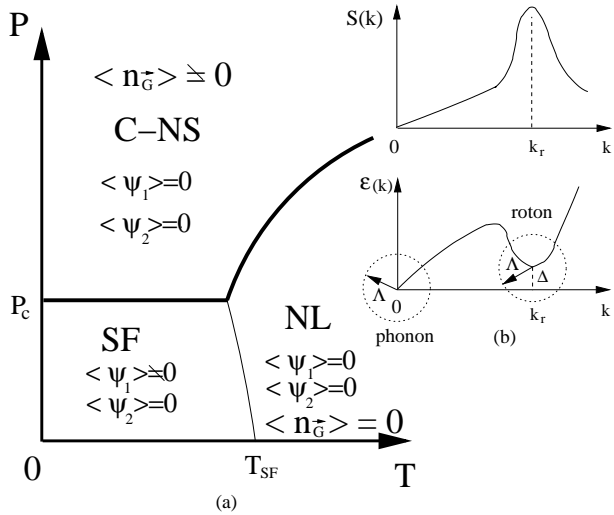


FIG. 1: (a) The theoretical phase diagram of GL model Eqns.1,2 and 3 in P versus T plane. This phase diagram only happens when $|g|$ is sufficiently small, so the normal solid is a C-NS (Fig.3). T controls thermal fluctuations, while p tunes quantum fluctuations. SF is the superfluid phase, C-NS is the commensurate normal solid phase which still does not have the P-H symmetry, it is likely to be a vacancy-like C-NS (NS-v). NL is the normal liquid phase. The supersolid phase is absent. Thick (thin) lines are 1st (2nd) order transitions. The critical temperatures T_{SF} of NL to SF transition drops slightly as the pressure p increases because of the quantum fluctuations. The SF to the C-NS transition is described by the QGL Eqn.11. (b) The structure factor and the separation of low (phonon) and high (roton) momenta regime in the dispersion relation in the SF. The Feynman relation between the two curves are explicitly derived in Eqn.9.

the roton minimum q_0 leads to the quantum Ginsburg-Landau action to describe the SF to the NS transition:

$$\mathcal{L}[\delta n] = \frac{1}{2}\delta n[A_n\omega_n^2 + r + c(q^2 - q_0^2)^2]\delta n - w(\delta n)^3 + u(\delta n)^4 + \dots \quad (11)$$

where $r \sim p_{c1} - p$ and $A_n \sim \frac{1}{\rho_s q_0^2}$ which is non-critical across the transition. Just like Eqn.1, because the instability happens at the finite wavevector $q = q_0$, Eqn.11 is *not a gradient expansion*, but an expansion in terms of the small order parameter δn . Again the average density n_0 does not appear in Eqn.11. The generic transition driven by the collapsing of roton minimum is from SF to NS instead of from the SF to the supersolid (SS). In the SF, $r > 0$, $\langle\psi\rangle \neq 0$, $\langle\delta n\rangle = 0$, In the NS, $r < 0$, $\langle\psi\rangle = 0$, $\langle\delta n\rangle = \sum_{\vec{G}}' n_{\vec{G}} e^{i\vec{G}\cdot\vec{x}}$ where \vec{G} are the shortest reciprocal lattice vector of the resulting lattice.

The corresponding phase diagram for the SF to the NS transition is shown in Fig.1.

In the Fig.1, even the SS does not exist as an equilibrium state, it may still exist as a metastable state which is interesting on its own, because it may have important

observable effects which will be discussed in Section IX. A similar 2 + 1 dimensional zero temperature excitonic superfluid to pseudo-spin density wave (PSDW) transition in bilayer quantum Hall system was worked out in⁴⁹.

III. SUPERFLUID TO SUPERSOLID TRANSITION AND GLOBAL PHASE DIAGRAM

In the last two sections, we discuss the SF to the SFDW transition with the order parameter ψ and the SF to the NS transition with the order parameter δn respectively. In this section, we discuss the SF to the SS transition with both order parameters ψ and δn . Then we have to also include the couplings between δn and ψ sector encoded in Eqn.3. The most difficult uncertainty in the SF-SFDW transition is to determine the lattice structure of the SFDW in the ψ sector which depends on microscopic details. Very fortunately, as shown in this section, this uncertainty disappears when the couplings Eqn.3 are taken into account, the SF to SFDW transition in the ψ sector becomes a SF to SS transition in the 4He system. Starting from the SF side with increasing pressure, we develop the theory based on the two facts (1) there is a roton minimum in the superfluid state (2) The instability to solid formation is driven by the gap diminishing at the roton minimum. The fact (1) was well established. The fact (2) also has some earlier theoretical and experimental supports (see^{22,23} and references therein). As shown in this last section, the fact (2) is guaranteed by the Feynman relation Eqn.4 which relates the roton minimum to the peak of the structure factor. Across the phase boundary $p = p_{c1}$ in Fig.2, the resulting solid could be an in-commensurate solid (IC-NS) with vacancies or interstitials even at $T = 0$ whose condensation leads to the formation of the SS-v and SS-i respectively where $\langle\psi\rangle \neq 0$ ^{2,3,15}. There is still some remanent of the SF in the IC-NS, the supersolid phase does exist as an equilibrium ground state. In this section, we assume $|g|$ is sufficiently large in Fig.2 and study the SF to the SS transition across $p = p_{c1}$. Because ψ is *also critical* through the transition, we can not simply integrate it out like in the last section. In fact, in the effective GL theory, we have to treat n and ψ on the same footing. From Eqn.1 and Eqn.2, we can see that n and ψ_2 have very similar propagators, so the lattice formation in n sector with $n(x) = n_0 + \sum_{\vec{G}}' n_{\vec{G}} e^{i\vec{G}\cdot\vec{x}}$ where $G = k_n$ and the superfluid density wave (SFDW) formation in ψ_2 sector with $\langle\psi_2(\vec{x})\rangle = e^{i\theta_2} \sum_{m=1}^P \Delta_m e^{i\vec{Q}_m \cdot \vec{x}}$ where $Q_m = k_r = k_n \sim 2\pi/a \sim 2\pi/3.17\text{\AA}$ have to happen simultaneously. From Hansen-Verlet criterion²⁵, when $S(k_n)/n_0$ is sufficiently large, solidification in the n sector occurs, so the roton minimum remains *finite* just before its condensation. The SFDW $\rho = |\psi_1 + \psi_2|^2$ is simply locked to (or commensurate with) the underlying normal solid (n) lattice. In fact, this locking is dictated by the ρ density- δn density couplings in Eqn.3. If the coupling g is attractive $g_v < 0$, the SFDW just

coincides with the n lattice. If it is repulsive $g_i > 0$, then it simply shifts the SFDW by suitable constants along the three unit vectors in the direct lattice. These constants will be determined in the next section for different n lattices. Namely, the supersolid states consist of two inter-penetrating lattices formed by the n lattice and the ψ_2 superfluid density wave. In fact, in a carefully prepared super-pressured sample, the roton minimum survives up to as high pressure as $p_r \sim 120$ bar. This fact suggests the roton minimum in the meta-stable state in a super-pressured sample is replaced by a SFDW which is commensurate with the n lattice in the stable SS state. Strikingly, this pressure $p_r \sim 120$ bar is close to $p_{c2} \sim 170$ bar in Fig.2 where the NCRI was extrapolated to vanish in the PSU's experiments¹⁰. This consistency also lead some support to the above picture. Obviously, when the pressure is so high that $p > p_{c2}$ in Fig.2, C-NS is the only possible ground state, any remnant of the SF completely disappears. So the vertical axis in the Fig.2 shows the SF-SS-NS series as the pressure P increases at $T = 0$

Combining the roton condensation picture²⁷ in the last section with the results reviewed in the introduction, we can sketch the following phase diagram Fig.2 of the complete QGL Eqns. 1, 2 and 3.

As can be seen from the Fig.2, starting from the SF side, as the pressure is increased at a given temperature, there are two possible states (1) At very low $T < T_{SS}$, the Bose-Einstein condensation (BEC) of ψ_2 leads to the supersolid state where $\langle \psi_1 \rangle \neq 0$, $\langle \psi_2 \rangle \neq 0$, $\langle n_{\vec{G}} \rangle \neq 0$. The instability happens at a finite wavevector $k = k_r$ instead of at $k = 0$. (2) At higher temperature $T_{SS} < T < T_{SF}$, there is a direct SF to NS transition. The SS state is certainly different from a conventional normal solid phase where $\langle \psi_1 \rangle = \langle \psi_2 \rangle = 0$, $\langle n_{\vec{G}} \rangle \neq 0$. In addition to the conventional translational and rotational orders characterized by ρ (which is the same as those characterized by n), the SS also has the ODLRO characterized by ψ_1 and ψ_2 . When decreasing the temperature at a given pressure, if $p < p_c$, the NL becomes SF at $T = T_{SF}$, the instability happens at $k = 0$. If $p > p_c$, the NL becomes a NS first at $T = T_m$, then there is a SFDW onset transition from the NS to a SS phase at $T = T_{SS}$. Starting from $T = 0$ and increasing the temperature, if $p < p_c$, the transition from the SF to the NL is driven by vortex unbindings; if $p > p_c$, the transition from the SS to the NS is also driven by the vortex unbinding in the global phase θ_2 (see Eqn.21), the phonon modes in the SS are non-critical across the transition, as the temperature increases further, the phonon modes drive the melting of the NS into the NL.

Because the SF to SS transition driven by the roton condensation can be either weakly or strong first order, in principle, Eqn.11 works precisely only in the SF side, it is not easy to study the precise nature of the SS state from the SF side. It turns out that it is more convenient to study the properties of the SS state from the NS side

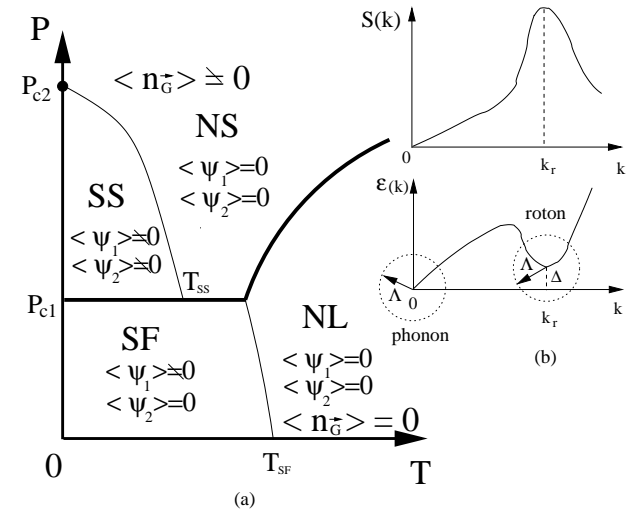


FIG. 2: (a) The theoretical phase diagram of GL model Eqns.1,2 and 3 in the pressure P versus temperature T plane. This phase diagram only happens when $|g|$ is sufficiently large (Fig.3). T controls thermal fluctuations, while p tunes quantum fluctuations. SF is the superfluid phase, NS is the normal solid phase, it is likely to be a vacancy-like normal solid (NS-v). NL is the normal liquid phase. The SS is likely to be the vacancies induced supersolid (SS-v). T_{SS} is an effective measurement of the strength of the coupling constant $g \neq 0$ in Eqn.3. Thick (thin) lines are 1st (2nd) order transitions. The critical temperatures of NL to SF and NS to SS transitions drop slightly as the pressure p increases because of the quantum fluctuations. The SF to the SS transition is a simultaneous combination of the SFDW transition in ψ sector driven by the roton condensation at $k_0 = k_r$ and the NS transition in the n sector driven by the divergence of the structure function at $k_0 = k_r = k_n$. (b) The structure factor and the separation of low (phonon) and high (roton) momenta regime in the SF.

in the next section. The results achieved from the NS side in the following section indeed confirm the roton condensation picture and the global phase diagram Fig.1.

IV. THE NORMAL SOLID TO THE SUPERSOLID TRANSITION

In this section, we approach the SS phase from the normal solid side and confirm it indeed exists and determine its lattice structure. Starting from the NS side, we show that the local tunneling processes in the NS-PH only leads to local fluctuations of ψ with a gap $\Delta(p)$ in Fig.3, so there is no long-range phase coherence and no supersolid in this case ($T_{SS} = 0$). Taking the NS-PH state as the reference state, we will show that if the coupling in Eqn.3 is sufficiently negative (or positive), the supersolids SS-v or SS-i can be realized by adding small number of vacancies to NS-v or interstitials to the NS-i (Fig.3). The attractive (repulsive) interaction is shown

to be crucial to raise the normal solid to the vacancy (interstitials) induced supersolid transition temperature T_{SS-v} (T_{SS-i}) above the zero temperature in the Fig.3. In fact, the temperature T_{SS} becomes an effective measure of the coupling strength g . We find that SS-v is more likely than SS-i. However, in order to be complete, we study both cases on the same footing. It is also constructive to compare SS-v with SS-i even though the SS-i is unlikely to be relevant to the Helium 4 system. When the two kinds of SS show different properties, we treat them differently, when they share the same properties, we treat them just in the same notation SS. The SS phase naturally and consistently fits into the phase diagram.

In the NL to the SF transition at $T = T_{XY} \sim 2.17K$, the BEC happens in the ψ_1 sector at $k = 0$, ψ_2 has a large gap and can be simply integrated out. In the NS, ψ stands for the vacancies or interstitials coming from the large zero point quantum fluctuations^{2,3,15}. Inside the NS, the translational symmetry is already broken, we can simply set $\delta n(\vec{x}) = n(\vec{x}) - n_0 = \sum'_{\vec{G}} n_{\vec{G}} e^{i\vec{G} \cdot \vec{x}}$ and put it into Eqn.3 to look at the effects of the coupling constants g and v . Imagine that at a given pressure $p > p_{c1} \sim 25$ bar, if tuning $g \rightarrow 0$, but keeping v intact, then the normal solid becomes an asymptotically P-H symmetric normal solid (NS-PH) in Fig.3. Inside the NL, the mass of ψ at $\vec{k} = 0$ is $t = T - T_{XY}$ which sets up the temperature scale of the problem. Inside the NS-PH, it is easy to see that the mass of ψ at $\vec{k} = 0$ is $t_{NS-PH} = t + v \sum'_{\vec{G}} |n(\vec{G})|^2$. If we take the temperature scale $t = T - T_{XY}$ as the reference scale, then $t_{NS-PH} = T + \Delta(p)$ where $\Delta(p) = v \sum'_{\vec{G}} |n(\vec{G})|^2 - T_{XY} > 0$ is the $T = 0$ gap for the local superfluid mode ψ at $\vec{k} = 0$ in the NS-PH. Because as the pressure p increases, the repulsive interaction v also increases, so it is reasonable to assume that $\Delta(p)$ is a monotonic increasing function of p . Because it is a first order transition across p_{c1} , just like the roton gap $\Delta_r > 0$ remains finite just before the first order transition, $\Delta(p)$ also remains finite just after the first order transition, namely, $\Delta(p_{c1}^+) > 0$ (Fig.3).

Taking this NS-PH as a reference state, we then gradually turn on g and see how the ground state evolves. In the presence of the periodic potential of $n(x)$ lattice, ψ will form a Bloch wave, the u interaction of ψ in Eqn.2 will certainly favor extended Bloch wave over strongly localized Wannier state. In principle, a full energy band calculation incorporating the interaction u is necessary to get the energy bands of ψ . Fortunately, qualitatively important physical picture of GL Eqns.1, 2, 3 can be achieved without such a detailed energy band calculation. We expect that the self interaction u only leads to some renormalization of the parameters t and K . Writing the g term in momentum space $g \sum_{\vec{G}} n(\vec{G}) \psi^*(\vec{G}) \psi(0)$ where $\vec{G} \neq 0$ and integrating out $\psi(\vec{G})$, we get a perturbative expansion on the eigen-energy $\epsilon_{\mu}(0)$ at the origin $\vec{K} = 0$, it is easy to see the n 's term is of the form $-(-g)^n$. Up

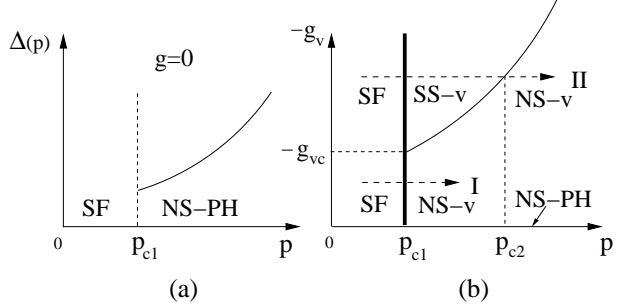


FIG. 3: (a) The gap $\Delta(p)$ of the local fluctuating superfluid mode ψ in the P-H symmetric commensurate normal solid (NS-PH) which exists only at $g = 0$. We assume it is a monotonic increasing function of the pressure p . (b) The zero temperature phase diagram of g_v verse the pressure p . The NS-PH only exists at $g_v = 0$. Any $g_v \neq 0$ will transfer the NS-PH into the NS-v. If the experimental is along the path I, then it is a direct 1st order SF to NS-v transition in Fig.1, if it is along the path II, it is a 1st order SF to SS-v, then a 2nd order SS-v to NS-v transition in Fig.2.

to the third order g_{μ}^3 , the series is:

$$\epsilon_{\mu}(0) = t_{NS-PH} - g_{\mu}^2 P \frac{n^2(\vec{G})}{K_{\mu} G^2} + g_{\mu}^3 \sum'_{\vec{G}_1} \sum'_{\vec{G}_2} \frac{n(\vec{G}_1) n(\vec{G}_2) n(-\vec{G}_1 - \vec{G}_2)}{K_{\mu} G_1^2 K_{\mu} G_2^2} + \dots \quad (12)$$

where the term linear in g vanishes, $\mu = v, i$ stands for vacancies and interstitials respectively and the shortest reciprocal lattice vector is $G = 2\pi/a$ with $a \sim 3.17\text{\AA}$ the lattice constant of the solid ${}^4\text{He}$, the $n(\vec{K}) = e^{-K^2 a^2 / 4\alpha}$ where K is any reciprocal lattice vector can be taken as a Gaussian where α is the width of the Gaussian.

In reality, $|g_v|$ maybe large, so we may need to go beyond leading order. For vacancies, $g_v < 0$, without writing out the coefficients explicitly, the expansion is

$$\epsilon_v(0) = t_{NS-PH} - g_v^2 - |g_v|^3 - |g_v|^4 - \dots \quad (13)$$

so the coefficient has the same sign. Assuming the series converges, for any $g_v < 0$, we can write $\epsilon_v(0) = t - f_v(g_v)$ where the $f_v(g_v) \geq 0$, $f_v(0) = 0$ is a monotonic increasing function of g_v and likely has no upper bound.

For interstitials, $g_i > 0$, without writing out the coefficients explicitly, the expansion is

$$\epsilon_i(0) = t_{NS-PH} - g_i^2 + g_i^3 - g_i^4 + \dots \quad (14)$$

so the coefficient has oscillating sign. Assuming the series converges, we can write $\epsilon_i(0) = t - f_i(g_i)$ which holds for any g_i . Because of the oscillating nature of the expansion coefficients, it is hard to judge the nature of the function of $f_i(g_i)$ except we are sure $f_i(0) = 0$. The different expansion series of $f_v(g_v)$ and $f_i(g_i)$ indicate that quantum fluctuations may favor vacancies over interstitials. However, for simplicity, we assume $f_i(g_i)$ is also a

monotonic increasing function of g_i , so we can discuss vacancies and interstitials induced supersolids on the same footing. In the following, we discuss SS-v and SS-i respectively.

A. Vacancies induced supersolid: SS-v

The mass of ψ_v was decreased to $t_{\psi_v} = T + \Delta(p) - f_v(g_v) = T - T_{SS-v}(p)$ where $T_{SS-v}(p) = f_v(g_v) - \Delta(p)$ (Fig.2). Because $f_v(g_v)$ is a monotonic increasing function of $|g_v|$ and $f_v(0) = 0$, defining a critical value $f_v(g_{vc}) = \Delta(p_{c1})$, then when $|g_v| < |g_{vc}|$, $f_v(g_v) < \Delta(p_{c1})$, the ψ_v mode remains massive, namely $\langle \psi_v \rangle = 0$. The C-NS remains to be the ground state even at $T = 0$. It is important to stress that even the solid is a C-NS, it still does not have the P-H symmetry. For $g_v < 0$, the C-NS is a vacancy-like C-NS (named as NS-v) where the vacancy excitation energy ϵ_v is lower than that of the interstitial ϵ_i (Fig.1b).

If $|g_v| > |g_{vc}|$, then $T_{SS-v}(p_{c1}) = f_v(g_v) - \Delta(p_{c1})$ is raised above the zero temperature, the SS-v state exists in the Fig.1b. $T_{SS-v}(p_{c1})$ is also proportional to the superfluid density measured in the experiments. The resulting solid is an in-commensurate solid with vacancies even at $T = 0$ whose condensation leads to $\langle \psi_v \rangle \neq 0$. Of course, the number of vacancies n_v is quite small. The SS-v state has a lower energy than the NS-v state at sufficiently low temperature. As the pressure increases to p_{c2} , $T_{SS-v}(p_{c2}) = f_v(g_v) - \Delta(p_{c2}) = 0$ (Fig.2). Then $f_v(g_v) = \Delta(p_{c2})$, so $T_{SS-v}(p) = \Delta(p_{c2}) - \Delta(p)$ which becomes an effective experimental measure of the energy gap $\Delta(p)$ in Fig.3a. Indeed, if reflecting the $\Delta(p)$ in Fig.3a with respect to the horizontal axis and then shift by $\Delta(p_{c2}) = f_v(g_v)$, then one recovers the $T_{SS-v}(p)$ in Fig.2. In the following, substituting the ansatz $\langle \psi_1(\vec{x}) \rangle = ae^{i\theta_1}$ and $\langle \psi_2(\vec{x}) \rangle = e^{i\theta_2} \sum_{m=1}^P \Delta_m e^{i\vec{Q}_m \cdot \vec{x}}$ where $Q_m = Q$ into Eqn.3, we study the effects of n lattice on $\psi = \psi_1 + \psi_2$. From Eqn.3, we can see $n(x)$ acts as a periodic potential on ψ . In order to get the lowest energy ground state, we must consider the following 4 conditions: (1) because any complex ψ (up to a global phase) will lead to local supercurrents which is costly, so we can take ψ to be real, so \vec{Q}_m have to be paired as anti-nodal points. P has to be even (2) as shown from the Feynman relation Eqn.4, $\vec{Q}_m, m = 1, \dots, P$ are simply P shortest reciprocal lattice vectors, then translational symmetry of the lattice dictates that $\epsilon(\vec{K} = 0) = \epsilon(\vec{K} = \vec{Q}_m)$, ψ_1 and ψ_2 have to condense at the same time (3) The point group symmetry of the lattice dictates $\Delta_m = \Delta$ and is real (4) for the vacancies case, the interaction is attractive $g_v < 0$, from Eqn.3, the SFDW-v simply sits on top of the n lattice, so the Superfluid Density wave $\rho = |\psi|^2$ simple sits on top of the n lattice as much as possible. This is reasonable, because vacancies are hopping on near the lattice sites, so the Bose condensation of vacancies also happen near the lattice sites. From Eqn.3, the attrac-

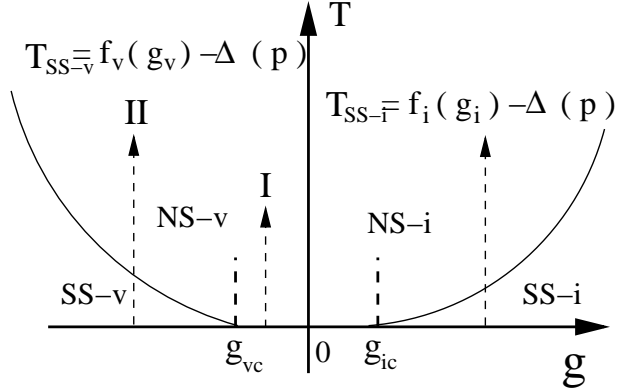


FIG. 4: The phase diagram of T versus g at a given pressure $p_{c1} < p < p_{c2}$. The finite temperature transitions denoted by the dashed line II at a given $|g_v| > |g_{vc}|$ (or $g_i > g_{ic}$) is in the 3D XY universality class described by Eqn.21. However, if $|g_v| < |g_{vc}|$, then the ground state at $T = 0$ is a vacancy-like C-NS(named as NS-v). Similar thing can be defined for an interstitial-like C-NS (named as NS-i) when $g_i < g_{ic}$.

tive interaction also favors $\psi(x = \vec{R}/2) \sim 0$ where $\vec{R}/2$ stands for any interstitial sites which are in the middle of lattice points. It turns out that the the 4 conditions can fix the relative phase and magnitude of ψ_1 and ψ_2 to be $\theta_2 = \theta_1$, $\Delta = a/P$, namely:

$$\psi_{ss-v} = \psi_0 \left(1 + \frac{2}{P} \sum_{m=1}^{P/2} \cos \vec{Q}_m \cdot \vec{x} \right) \quad (15)$$

where $\psi_0 = ae^{i\theta}$ depends on the temperature and pressure. Note that in contrast to a uniform superfluid, the magnitude of ψ is changing in space. This field satisfies the Bloch theorem with the crystal momentum $\vec{k} = 0$ and the Fourier components are $\psi(\vec{K} = 0) = a$, $\psi(\vec{K} = \vec{Q}_m) = a/P$. They have the same sign and decay in magnitude. In principle, higher Fourier components may also exist, but they decay very rapidly, so can be neglected without affecting the physics qualitatively.

B. Interstitial induced supersolid: SS-i

The discussion is quite similar to the vacancy case except that (1) if $g_i < g_{ic}$, the C-NS is an interstitial-like C-NS (named as NS-i) where the interstitial excitation energy ϵ_i is lower than that of the vacancy ϵ_v (2) if $g_i > g_{ic}$, the resulting solid is an in-commensurate solid with interstitials even at $T = 0$ whose condensation leads to $\langle \psi_i \rangle \neq 0$, the SS-i state exists in the Fig.2. The arguments to determine the lattice structure of the SS-i goes the same as those in the vacancies case except the condition (4), for the SS-v, the interaction is attractive $g_v < 0$, the SFDW-v simply sits on top of the n lattice. However, for the interstitials case, the interaction is repulsive $g_i > 0$ favors $\psi(x = 0) \sim 0$, so the Superfluid

Density wave $\rho = |\psi|^2$ can avoid the n lattice as much as possible. This is reasonable, due to the competing of the two orders, the superfluid component emerges from the places where the normal solid component is suppressed. It turns out that the the 4 conditions can fix the relative phase and magnitude of ψ_1 and ψ_2 to be $\theta_2 = \theta_1 + \pi, \Delta = a/P$, namely:

$$\psi_{ss-i} = \psi_0 \left(1 - \frac{2}{P} \sum_{m=1}^{P/2} \cos \vec{Q}_m \cdot \vec{x}\right) \quad (16)$$

where $\psi_0 = ae^{i\theta}$ depends on the temperature and pressure. Note that the crucial sign difference from the vacancies case which make an important difference from the X-ray scattering from SS-v and SS-i to be discussed in the next section. Again in contrast to a uniform superfluid, the magnitude of ψ is changing in space. This field satisfies the Bloch theorem with the crystal momentum $\vec{k} = 0$ and the Fourier components are $\psi(\vec{K} = 0) = a, \psi(\vec{K} = \vec{Q}_m) = -a/P$. They oscillate in sign and decay in magnitude. In principle, higher Fourier components may also exist, but they decay very rapidly, so can be neglected without affecting the physics qualitatively.

In the following, we will discuss different lattice structures of n when $P = 2, 4, 6, 8, 12$ respectively. Obviously, the Superfluid Density wave $\rho = |\psi|^2$ has the same Bravais lattice structure as the the n lattice. However, as shown in the following, even n is a Bravais lattice, the SFDW may be the same Bravais lattice plus a few basis.

(a) P=2: $\vec{Q}_1 = -\vec{Q}_2 = \vec{Q}$ are a pair of anti-nodal points. They are the two shortest reciprocal lattice vectors generating a 1 dimensional lattice embedded in a 3 dimensional system. The field is $\psi(\vec{x}) = a(1 - \cos \vec{Q} \cdot \vec{x})$. There is a superfluid density wave formation transition inside the normal solid which is a 2nd order transition in the universality class of 3D XY model(Fig.2). The local SFDW operator $\rho_s^l = |\psi(\vec{x})|^2 = a^2(1 - \cos \vec{Q} \cdot \vec{x})^2$. It breaks translational invariance only along 1-dimension which is similar to Smectic-A or Smectic-C phase in the liquid crystal²⁵. The maxima of the SFDW $\psi_{max} = 2a$ appear exactly in the middle of lattice points at $\vec{a} = \frac{1}{2}\vec{a}_1$. So the SFDW forms the dual lattice of the 1d lattice which is also a 1d lattice.

(b) P=4: $\vec{Q}_3 = -\vec{Q}_1, \vec{Q}_4 = -\vec{Q}_2, \vec{Q}_1 \cdot \vec{Q}_2 = 0, \vec{Q}_i, i = 1, 2, 3, 4$ form the 4 corners of a square. They are the four shortest reciprocal lattice vectors generating a 2 dimensional square lattice embedded in a 3 dimensional system. The field is $\psi(\vec{x}) = a[1 - \frac{1}{2}(\cos \vec{Q}_1 \cdot \vec{x} + \cos \vec{Q}_2 \cdot \vec{x})]$, The local SFDW operator $\rho_s^l = |\psi(\vec{x})|^2$. The maxima of the SFDW $\psi_{max} = 2a$ appear exactly in the middle of lattice points at $\vec{a} = \frac{1}{2}(\vec{a}_1 + \vec{a}_2)$. So the SFDW forms the dual lattice of the square lattice which is also a square lattice.

(c) P=6: there are two cases need to be discussed separately. (c1) $\vec{Q}_i, i = 1, 2, 3, 4, 5, 6$ form the 6 corners of a hexagon. They consist of the 6 shortest reciprocal lat-

tice vectors generating a 2 dimensional triangular lattice embedded in a 3 dimensional system. The field is $\psi(\vec{x}) = a[1 - \frac{1}{3}(\cos \vec{Q}_1 \cdot \vec{x} + \cos \vec{Q}_2 \cdot \vec{x} + \cos \vec{Q}_3 \cdot \vec{x})]$. The maxima of the SFDW $\psi_{max} = 3/2a$ appear in the middle of lattice points at $\vec{a} = \pm \frac{1}{3}(\vec{a}_1 + \vec{a}_2)$. They form the *dual* lattice of the triangular lattice which is a honeycomb lattice. The honeycomb lattice is not a Bravais lattice which has two triangular sublattices *A* and *B*, it can be considered as one triangular lattice *A* plus a basis. This can be understood intuitively: there are two equivalent ways to shift the n lattice, one way to get the sublattice *A*, the other to get the sublattice *B*. Putting *A* and *B* together forms the SFDW which takes the honeycomb lattice (c2) $\vec{Q}_i, i = 1, 2, 3, 4, 5, 6$ are the 6 shortest reciprocal lattice vectors generating a cubic lattice. The maxima of the SFDW $\psi_{max} = 2a$ appear exactly in the middle of lattice points at the 8 points $\vec{a} = \frac{1}{2}(\pm \vec{a}_1 \pm \vec{a}_2 \pm \vec{a}_3)$. So the SFDW forms the dual lattice of the cubic lattice which is also a cubic lattice.

(d) $P = 8$: $\vec{Q}_i, i = 1, \dots, 8$ form the 8 shortest reciprocal lattice vectors generating a *bcc* reciprocal lattice which corresponds to a *fcc* direct lattice. The field is $\psi(\vec{x}) = a[1 - \frac{1}{4}(\cos \vec{Q}_1 \cdot \vec{x} + \cos \vec{Q}_2 \cdot \vec{x} + \cos \vec{Q}_3 \cdot \vec{x} + \cos \vec{Q}_4 \cdot \vec{x})]$. The maxima of the SFDW $\psi_{max} = 2a$ appear in all the edge centers such as $(1/2, 0, 0)$ etc. and the centers of any cube such as $(1/2, 1/2, 1/2)$ etc. It is easy to see these points can be achieved by simply shifting the n lattice by $(1/2, 1/2, 1/2)$, so the SFDW also forms a *fcc* direct lattice.

(e) $P = 12$: $\vec{Q}_i, i = 1, \dots, 12$ form the 12 shortest reciprocal lattice vectors generating a *fcc* reciprocal lattice which corresponds to a *bcc* direct lattice. The field is $\psi(\vec{x}) = a[1 - \frac{1}{6}(\cos \vec{Q}_1 \cdot \vec{x} + \cos \vec{Q}_2 \cdot \vec{x} + \cos \vec{Q}_3 \cdot \vec{x} + \cos \vec{Q}_4 \cdot \vec{x} + \cos \vec{Q}_5 \cdot \vec{x} + \cos \vec{Q}_6 \cdot \vec{x})]$. The maxima of the SFDW $\psi_{max} = 4/3a$ appear along any square surrounding the center of the cube such as $(1/2, \beta, 0)$ or $(1/2, 0, \gamma)$ etc. In fact, one can achieve the SFDW lattice by shifting the the center of *bcc* to the 3 face centers, so all these points are on the edge centers and face centers which are only discrete points on the square surrounding the center of the cube. We expect the continuous whole square is due to the artifact of the approximation $\psi(x = 0) \sim 0$ imposed. So the SFDW 4He in Vycor glass takes a *bcc* lattice.

Unfortunately, a spherical $k = Q$ surface can not lead to lattices with different lengths of primitive reciprocal lattice vectors such as a *hcp* lattice. This is similar to the classical liquid-solid transition described by Eqn.1 where a single maximum peak in the static structure factor can not lead to a *hcp* lattice²⁵. Another difficulty with the *hcp* lattice is that the *hcp* lattice is not a Bravais lattice, it consist of two inter-penetrating simple hexagonal lattices shifted by $\vec{a} = \frac{1}{3}\vec{a}_1 + \frac{1}{3}\vec{a}_2 + \frac{1}{2}\vec{a}_3$. Here we can simply take the experimental fact that n forms a *hcp* lattice without knowing how to produce such a lattice from a GL theory Eqn.1. Despite the technical difficulty, because for an idea *hcp* lattice $c/a = \sqrt{8/3}$, an *hcp* lattice has 12 nearest

neighbors, so its local environment may resemble that of an *fcc* lattice. We expect the physics (except the anisotropy of NCRI in the *hcp* lattice to be discussed in the next two sections) is qualitatively the same as that in *fcc* direct lattice. From the insights achieved from the other lattices, one can achieve the SFDW lattice by shifting the *hcp* lattice of n by $\vec{a} = \frac{2}{3}(\vec{a}_1 + \vec{a}_2) + \frac{1}{4}\vec{a}_3$.

C. Discussions on both SS-v and SS-i

In fact, for both SS-v and SS-i, we can write n and ψ sector in a more symmetric way: $n(\vec{x}) = n_0 + \sum'_{\vec{G}} n_{\vec{G}} e^{i\vec{G}\cdot\vec{x}}, \psi(\vec{x}) = \psi_0 + \sum'_{\vec{G}} \psi_{\vec{G}} e^{i\vec{G}\cdot\vec{x}}$. It is easy to see that in the SS, the translational symmetry $\vec{x} \rightarrow \vec{x} + \vec{a}, n_{\vec{G}} \rightarrow n_{\vec{G}} e^{i\vec{G}\cdot\vec{a}}, \psi_{\vec{G}} \rightarrow \psi_{\vec{G}} e^{i\vec{G}\cdot\vec{a}}$ is broken down to $\vec{a} = \vec{R}, n_{\vec{G}} \rightarrow n_{\vec{G}} e^{i\vec{G}\cdot\vec{R}} = n_{\vec{G}}, \psi_{\vec{G}} \rightarrow \psi_{\vec{G}} e^{i\vec{G}\cdot\vec{R}} = \psi_{\vec{G}}$. In the Fig.2, in the NL side, as the temperature is lowered, the symmetry breaking happens in ψ_1 at $k = 0$, the NL gets into the SF. However, as shown in this section, in the NS side, the symmetry breaking happens in both the ψ_1 at $k = 0$ and ψ_2 sector at P discrete points in a spherical surface $k = Q$ simultaneously, the NS gets to the SS state at a much lower critical temperature T_{SS} . The results achieved from the NS side in this section indeed confirm Fig.2 achieved from the roton condensation picture in the SF phase in the last section.

V. THE ZERO TEMPERATURE TRANSITION FROM NS TO SS DRIVEN BY THE PRESSURE

The analysis so far focused on finite temperature and mean field level. Some interesting physics near the *finite temperature* NS to SS transition in Fig.1 was explored in¹⁴ by considering the coupling of elastic degree of freedoms to the SF mode. For example, the sound velocity will acquire a dip similar to the specific heat cusp in the λ transition in superfluid Helium. In this and following sections, I will push the Ginsburg-Landau (GL) theory in the previous sections to zero temperature and to include all the possible low energy fluctuations above the mean field solutions achieved in the previous sections. Particularly, I will work out the new elementary low energy excitations including vortex loop excitations in a SS and study how they defer from the low energy excitations in solids and superfluids. In principle, if these elementary low energy excitations can be detected by X-ray scattering, neutron scattering, acoustic wave attenuation and heat capacity experiments in solid Helium 4 can prove or disprove the existence of the supersolid in Helium 4. In practice, the detection may still be complicated by sample quality. No matter if a supersolid indeed exists in Helium 4, these results should be interesting in its own and may have application in other systems.

So far, we only look at the mean field solutions corresponding to vacancies and interstitials. Here we discuss

excitations above the mean field solutions. It turns out that the excitations in both cases are the same, so we discuss both cases at same time. In the SS-v and SS-i, the wavefunctions can be written as

$$\psi_{ss} = \psi_0(1 \pm \frac{2}{P} \sum_{m=1}^{P/2} \cos \vec{Q}_m \cdot \vec{x}), \quad \psi_0 = |\psi_0| e^{i\theta} \quad (17)$$

where \pm sign corresponds to SS-v and SS-i respectively. Obviously, there are also topological defects in the phase winding of θ which are vortices. At $T \ll T_{SS}$, the vortices can only appear in tightly bound pairs. However, as $T \rightarrow T_{SS}^-$, the vortices start to become liberated, this process renders the total NCRI to vanish above $T > T_{SS}$. In addition to the superfluid θ mode in SS states, there are also lattice phonon modes \vec{u} in both n sector and ψ_2 sector. However, it is easy to see that the coupling Eqn.3 is invariant under $\vec{x} \rightarrow \vec{x} + \vec{u}, n(\vec{G}) \rightarrow n(\vec{G}) e^{i\vec{G}\cdot\vec{u}}, \psi(\vec{G}) \rightarrow \psi(\vec{G}) e^{i\vec{G}\cdot\vec{u}}$, so the lattice phonon modes in ψ are locked to those in the conventional n lattice. This is expected because there is only one kind of translational symmetry breaking, therefore only one kind of lattice phonons. Inside the NS side, the translational symmetry is already broken, so we can parameterize the density deviation order parameter $\delta n(\vec{x}, \tau) = n(\vec{x}, \tau) - n_0$ and the SF complex order parameter $\psi(\vec{x}, \tau)$ as:

$$\begin{aligned} \delta n(\vec{x}, \tau) &= \sum'_{\vec{G}} n_{\vec{G}} e^{i\vec{G}\cdot(\vec{x} + \vec{u}(\vec{x}, \tau))} \\ \psi(\vec{x}, \tau) &= \psi_0(\vec{x}, \tau) [1 \pm \frac{1}{P} \sum'_{\vec{G}} e^{i\vec{G}\cdot(\vec{x} + \vec{u}(\vec{x}, \tau))}] \end{aligned} \quad (18)$$

where \pm means vacancy or interstitials induced supersolids respectively, $n_{\vec{G}}^* = n_{-\vec{G}}$ the " " means the sum over the shortest non-zero reciprocal lattice vector \vec{G} and P is the number of them, the $\vec{u}(\vec{x}, \tau)$ are the 3 lattice phonon modes, the $\psi_0(\vec{x}, \tau) = |\psi_0(\vec{x}, \tau)| e^{i\theta(\vec{x}, \tau)}$ is the SF order parameter. From Eqn.18, we can identify the SS density order parameter $\rho_{\vec{G}}(\vec{x}, \tau) = e^{i\vec{G}\cdot\vec{u}(\vec{x}, \tau)}$. The effective action to describe the NS to SF transition at $T = 0$ consistent with all the lattice symmetries and the global $U(1)$ symmetry is:

$$\begin{aligned} \mathcal{L} = & \psi_0^\dagger \partial_\tau \psi_0 + c_{\alpha\beta} \partial_\alpha \psi_0^\dagger \partial_\beta \psi_0 + r |\psi_0|^2 + g |\psi_0|^4 \\ & + \frac{1}{2} \rho_n (\partial_\tau u_\alpha)^2 + \frac{1}{2} \lambda_{\alpha\beta\gamma\delta} u_{\alpha\beta} u_{\gamma\delta} \\ & + a_{\alpha\beta}^0 u_{\alpha\beta} \psi_0^\dagger \partial_\tau \psi_0 + a_{\alpha\beta}^1 u_{\alpha\beta} |\psi_0|^2 + \dots \end{aligned} \quad (19)$$

where $r = p - p_{c2}$ with $p_{c2} \sim 170$ bar (Fig. 1), ρ_n is the normal density, $u_{\alpha\beta} = \frac{1}{2}(\partial_\alpha u_\beta + \partial_\beta u_\alpha)$ is the strain tensor, $\lambda_{\alpha\beta\gamma\delta}$ are the bare elastic constants dictated by the symmetry of the lattice, it has 5 (2) independent elastic constants for a *hcp* (isotropic) lattice. For a uniaxial lattice such as *hcp* lattice, all the coefficients $c_{\alpha\beta}, a_{\alpha\beta}^0, a_{\alpha\beta}^1$ take the same form $c_{\alpha\beta} = c_z n_\alpha n_\beta + c_\perp (\delta_{\alpha\beta} - n_\alpha n_\beta)$ where

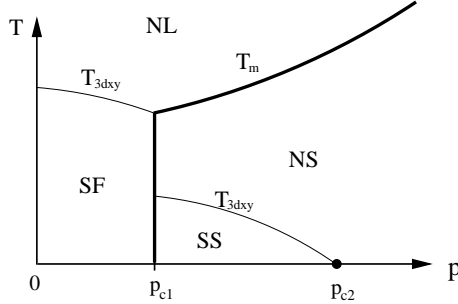


FIG. 5: Possible temperature T versus pressure p phase diagram of Helium 4. SF is the superfluid phase, SS is the supersolid phase, NS is the normal solid phase, NL is the normal liquid phase. T_{3dxy} is the 3d XY transition. T_m is the 1st order melting transition. The dot is the zero temperature transition from the NS to the SS which is a transition with mean field exponents $z = 2, \nu = 1/2, \eta = 0$. Thick (thin) line is 1st (2nd) order transition. This figure can be obtained from Fig.2 by rotating 90°.

\vec{n} is a unit vector along the uni-axis^{14,33}. In the NS state $r > 0$, $\langle \psi_0(\vec{x}, \tau) \rangle = 0$, the 3 lattice phonon modes $\vec{u}(\vec{x}, \tau)$ become the 3 ordinary ones. While inside the SS state $r < 0$, $\langle \psi_0(\vec{x}, \tau) \rangle \neq 0$. From the parameterizations of $\psi(\vec{x}, \tau)$, we can see if the prefactor $\langle \psi_0(\vec{x}, \tau) \rangle \neq 0$, then $\psi(\vec{x}, \tau)$ condenses at both $\vec{G} = 0$ and any other non-zero reciprocal lattice vectors \vec{G} to form the superfluid density wave (SFDW) $\rho_l^s = |\psi(\vec{x}, \tau)|^2$ inside the SS. The $a_{\alpha\beta}^0$ and $a_{\alpha\beta}^1$ couplings come from the original couplings $\delta n(\vec{x}, \tau) \psi^\dagger \partial_\tau \psi$ and $\delta n(\vec{x}, \tau) |\psi|^2$ respectively in the GL in Sect.I. If setting all the couplings between ψ_0 and u_α vanish, the ψ_0 sector describes the SF to Mott insulator transition in a *rigid* underlying lattice³⁵. So we can also view this project as to study how the NS to SS transition at $T = 0, p = p_{c2}$ in a rigid lattice is affected by its coupling to a quantum fluctuating lattice. Under the Renormalization group (RG) transformation, $\tau' = \tau/b^z, x' = x/b$ and $\psi' = \psi/Z$. If we choose $z = 2, Z = b^{-d/2}$, the $g' = gb^{2-d}$. It is well known that the SF to Mott insulator transition in a *rigid* underlying lattice has the mean field exponents with $z = 2, \nu = 1/2, \eta = 0$ at $d \geq 2$ ³⁵. We also choose $u'_\alpha = u_\alpha/Z$, then $\rho'_s = b^{-2} \rho_n$, so the lattice phonon kinetic energy term is irrelevant near the QCP. It is easy to see $a'_0 = b^{-d/2-1} a_0$, so a_0 is always irrelevant. $a'_1 = b^{1-d/2} a_1$, so both g and a_1 's upper critical dimension is $d_u = 2$, so, in principle, a $\epsilon = 2 - d$ expansion is possible for both g and a_1 . However, both are irrelevant at $d = 3$. We conclude that NS to SS transition at $T = 0$ remains the same as that in a rigid lattice described by

$$\mathcal{L}_{T=0} = \psi_0^\dagger \partial_\tau \psi_0 + c_{\alpha\beta} \partial_\alpha \psi_0^\dagger \partial_\beta \psi_0 + r |\psi_0|^2 + g |\psi_0|^4 + \dots \quad (20)$$

Namely, it is a transition with mean field exponents $z = 2, \nu = 1/2, \eta = 0$.

If neglecting the τ dependence by setting $u_\alpha(\vec{x}, \tau) = u_\alpha(\vec{x})$, $\psi_0(\vec{x}, \tau) = \psi_0(\vec{x})$, then Eqn.19 reduces to the classical action studied in^{14,33}. For the classical case, $x' =$

$x/b, \psi' = \psi/Z, u'_\alpha = u_\alpha/Z$, if we choose $Z = b^{(2-d)/2}$, then $g' = gb^{4-d}, a'_1 = b^{2-d/2} a_1$, so both g and a_1 's upper critical dimension is $d_u = 4$. So in principle, a $\epsilon = 4 - d$ expansion is possible for both g and a_1 , the putting $\epsilon = 1$ for $d = 3$. In³³, it was shown that due to the specific heat exponent of the 3d XY model $\alpha = -0.012 < 0$, the $a_{\alpha\beta}^1$ coupling is irrelevant, so the NS to SS transition remains to be a classical 3d XY transition at finite temperature given by:

$$\mathcal{L}_T = K_{NS} |\nabla \psi_0|^2 + t_{NS} |\psi_0|^2 + u_{NS} |\psi_0|^4 + \dots \quad (21)$$

where $t_{NS} = T - T_{SS}$ and $T_{SS-v}(p) = f_v(g_v) - \Delta(p) = \Delta(p_{c2}) - \Delta(p)$ and $T_{SS-i}(p) = f_i(g_i) - \Delta(p) = \Delta(p_{c2}) - \Delta(p)$. Obviously, it is still a 3d XY transition. It was shown in¹⁴ that the coupling to the phonon mode \vec{u} will not change the universality class at finite temperature. As the pressure increased to p_{c2} , T_{SS-v} or T_{SS-i} are suppressed to zero, the system becomes a C-NS where $\langle \psi \rangle = 0$. It is important to stress that even at $p > p_{c2}$, the solid is a C-NS, it still does not have the P-H symmetry because $g \neq 0$. For $g_v < 0$, the C-NS is vacancy like (NS-v) where the vacancy excitation energy is lower than that of the interstitial. For $g_i > 0$, the C-NS is interstitial like (NS-i) where the interstitial excitation energy is lower than that of the vacancy.

VI. THE NCRI OF SF AND SS STATES AT $T = 0$ AND $T > 0$.

In order to calculate the superfluid density ρ_s explicitly, we need to look at how the system's free energy responses to a fictitious gauge potential \vec{A} . We find that when $\Delta \gg \Delta_c$, $\rho_s(T = 0) = \rho = \int d^d x |\psi(\vec{x}, \tau)|^2 = \int d^d x (|\psi_1(\vec{x}, \tau)|^2 + |\psi_2(\vec{x}, \tau)|^2)$ where the crossing terms between ψ_1 and ψ_2 drop out due to the momenta conservation. Note that although ψ_2 does not contribute to the condensate, it does contribute to the superfluid density. This is consistent with the fact that although 90% 4He are out of the condensate, they all contribute to the superfluid density.

In the SF state, at low T , the quantum fluctuations induced by the pressure are important. Let's first look at the quantum phase fluctuations. The phase fluctuation action is given by $\mathcal{L}_p = \frac{1}{2g} \frac{1}{\beta} \sum_{i\omega_n} \int \frac{d^d k}{(2\pi)^d} (\omega_n^2 + k^2) |\theta(\vec{k}, \omega_n)|^2$ where $g = \frac{1}{\rho_s}$ controls the strength of quantum phase fluctuations and the superfluid phonon velocity has been set equal to 1 for simplicity. It is easy to see that at $T = 0$, $\langle \theta^2(\vec{x}, \tau) \rangle_{T=0}$ is infra-red (IR) finite, so the quantum phase fluctuations alone will not lead to any instability. However, it will lead to superfluid density depletion even before reaching the phase boundary of SF to SS transition in Fig.1 and Fig.2, although the depletion may be quite small. This fact explains why $T_{SF}(p)$ bends to the left slightly as the pressure p increases. At finite T , the thermal fluctuations $\langle \theta^2(\vec{x}, \tau) \rangle_T - \langle \theta^2(\vec{x}, \tau) \rangle_{T=0} \sim T^{d-1}$ lead to $\rho_s(T) =$

$\rho_s(T=0) - cT^2$ at $d=3$. It is well known the superfluid density $\rho(T) \sim \rho(T=0) - aT^4$, while the Bose condensation density $n_b(T) \sim n_b(T=0) - bT^2$. So strictly speaking, ψ sector can only describe the bose condensation density. This is expected, because the n sector in the SF phase also contributes to the superfluid density, but not to the BEC.

Then let's look at the roton fluctuations. Setting $\Delta_2 = \Delta^2$, at $T=0$, the quantum roton fluctuations $\langle \phi_2^2(\vec{x}, \tau) \rangle_{T=0} \sim \log \frac{\Lambda}{\Delta}$ is IR logarithmic divergent as $\Delta \rightarrow 0$ which signifies the instability to the lattice formation. Due to this IR divergence, the 1st order SF to SS transition may happen well before Δ becomes zero, namely, at $\Delta = \Delta_c > 0$. This is consistent with the picture described in sec. IV. At finite T , the thermal roton fluctuations $\langle \phi_2^2(\vec{x}, \tau) \rangle_T - \langle \phi_2^2(\vec{x}, \tau) \rangle_{T=0} \sim (\log \frac{\Lambda}{\Delta}) e^{-\frac{\Delta}{T}}$ when $T \ll \Delta \ll \Lambda$.

In the SS-v and SS-i states, the $n(x)$ forms a lattice, at the same time, the unstable roton part is replaced by a stable SFDW formation commensurate with the underlying n lattice. Obviously, the $n(x)$ normal lattice takes away the vast majority of density from the superfluid density even at $T=0$. It can be shown that superfluid density from the ψ_1 sector is isotropic $\rho_1 \sim Ka^2$, while the superfluid density from ψ_2 sector turns out to anisotropic in *hcp* lattice $\rho_{2,ij} \sim \sum_{m=1}^P |\Delta_m|^2 Q_{mi} Q_{mj} / Q^2$ where $\Delta_m = \pm a/P$ for SS-v or SS-i. Therefore, the total superfluid density in SS phase is:

$$\rho_{ij}^{SS} \sim \rho_1 \delta_{ij} + \rho_{2,ij} \sim a^2 (K \delta_{ij} + \frac{1}{P^2} \sum_{m=1}^P Q_{mi} Q_{mj} / Q^2) \quad (22)$$

Taking $P=6$, the anisotropy is quite small. Solid 4He in a bulk takes a *hcp* lattice with $c/a \sim 1.63$ which is quite close to the idea value $c/a = \sqrt{8/3}$. The three primitive reciprocal lattice vectors are $G_1 = G_2 = \frac{4\pi}{\sqrt{3}a}$, $G_3 = \frac{2\pi}{c}$. We can estimate the anisotropy of the NCRI in the *hcp* lattice. If the rotation axis is along the c axis, the NCRI is $\rho_{11} \sim Ka^2 + v_r \sum_{m=1}^6 |\Delta_m|^2 Q_{m1} Q_{m1} / Q^2$. If the rotation axis is along the a (or b) axis, the NCRI is $\rho_{33} \sim Ka^2 + v_r \sum_{m=1}^6 |\Delta_m|^2 Q_{m3} Q_{m3} / Q^2$. The anisotropy mainly comes from the ψ_2 sector. Setting $s = G_1/G_3$, for the idea value $s = \frac{4\sqrt{2}}{3} > 1$, so $\rho_{11} > \rho_{33}$. Namely, the NCRI response is larger when one is rotating the sample around the c axis than that when one is rotating the sample around the a or b axis. However, as the pressure is increased, s decreases, the anisotropy of the NCRI also decreases. In the PSU experiments, the samples are poly-crystal, the relative orientation of the rotation axis to the c axis is not known, so it's hard to test this prediction with poly-crystals.

VII. NON-TOPOLOGICAL ELEMENTARY EXCITATIONS IN THE SS

Classical non-equilibrium hydrodynamics in SS was investigated for a long time^{2,34}. These hydrodynamics will break down at very low temperature where quantum fluctuations dominate. However, the quantum nature of the excitations in the SS has not been studied yet. Here, we will study the quantum characteristics of low energy excitations in the SS. For example, how the phonon spectra in the SS differ from that in a NS and how the SF mode in the SS differs from that in a SF. Inside the SS, $\langle \psi_0(\vec{x}, \tau) \rangle = a$, we can write $\psi_0(\vec{x}, \tau) = \sqrt{a + \delta\rho} e^{i\theta(\vec{x}, \tau)}$ and plug it into the Eqn.19:

$$\begin{aligned} \mathcal{L} = & i\delta\rho\partial_\tau\theta + \rho_{\alpha\beta}^s\partial_\alpha\theta\partial_\beta\theta + \frac{1}{2}\delta\rho S_0^{-1}\delta\rho \\ & + \frac{1}{2}[\rho_n(\partial_\tau u_\alpha)^2 + \lambda_{\alpha\beta\gamma\delta} u_{\alpha\beta} u_{\gamma\delta}] \\ & + a_{\alpha\beta}^0 u_{\alpha\beta} i\partial_\tau\theta + a_{\alpha\beta}^1 u_{\alpha\beta} \delta\rho + \dots \end{aligned} \quad (23)$$

where we already dropped $i\partial_\tau\theta$ term which is irrelevant inside the SS phase (although it is very important in describing the $T=0$ NS to SS transition discussed in the last section), S_0 is the bare density-density correlation function. Integrating out the massive magnitude $\delta\rho$ fluctuations, we get:

$$\begin{aligned} \mathcal{L} = & -\frac{S_0}{2}(i\partial_\tau\theta + a_{\alpha\beta}^1 u_{\alpha\beta})^2 + \rho_{\alpha\beta}^s\partial_\alpha\theta\partial_\beta\theta \\ & + \frac{1}{2}[\rho_n(\partial_\tau u_\alpha)^2 + \lambda_{\alpha\beta\gamma\delta} u_{\alpha\beta} u_{\gamma\delta}] \\ & + a_{\alpha\beta}^0 u_{\alpha\beta} i\partial_\tau\theta + \dots \end{aligned} \quad (24)$$

Expanding the square, we get the effective action describing the low energy modes inside the SS phase:

$$\begin{aligned} \mathcal{L} = & \frac{1}{2}[\kappa(\partial_\tau\theta)^2 + \rho_{\alpha\beta}^s\partial_\alpha\theta\partial_\beta\theta] \\ & + \frac{1}{2}[\rho_n(\partial_\tau u_\alpha)^2 + \lambda_{\alpha\beta\gamma\delta} u_{\alpha\beta} u_{\gamma\delta}] + a_{\alpha\beta} u_{\alpha\beta} i\partial_\tau\theta \end{aligned} \quad (25)$$

where κ is the SF compressibility and $\rho_{\alpha\beta}^s$ is the SF stiffness which has the same symmetry as $a_{\alpha\beta}^0$, $a_{\alpha\beta} = a_{\alpha\beta}^0 + S_0 a_{\alpha\beta}^1$ where $S_0(\vec{k}, \omega)$ is the bare SF density correlation function. Obviously, the last term is the crucial coupling term which couples the lattice phonon modes to the SF mode. The factor of i is important in this coupling. By integration by parts, this term can also be written as $a_{\alpha\beta}(\partial_\tau u_\beta \partial_\alpha\theta + \partial_\tau u_\alpha \partial_\beta\theta)$ which has the clear physical meaning of the coupling between the SF velocity $\partial_\alpha\theta$ and the velocity of the lattice vibration $\partial_\tau u_\beta$. It is this term which makes the low energy modes in the SS to have its own characteristics which could be detected by experiments. In this section, we neglect the topological vortex loop excitations in Eqn.23. In the next section, we will discuss these vortex loop excitations in detail. In the following, we discuss two extreme cases: isotropic solid and *hcp* lattice separately. Usual samples are between the two extremes.

A. Isotropic solid

A truly isotropic solid can only be realized in a highly poly-crystalline sample. Usual samples are not completely isotropic. However, we expect the simple physics brought about in an isotropic solid may also apply qualitatively to other samples which is very poly-crystalline.

For an isotropic solid, $\lambda_{\alpha\beta\gamma\delta} = \lambda\delta_{\alpha\beta}\delta_{\gamma\delta} + \mu(\delta_{\alpha\gamma}\delta_{\beta\delta} + \delta_{\alpha\delta}\delta_{\beta\gamma})$ where λ and μ are Lame coefficients, $\rho_{\alpha,\beta}^s = \rho^s\delta_{\alpha,\beta}$, $a_{\alpha,\beta} = a\delta_{\alpha,\beta}$. In (\vec{q}, ω_n) space, Eqn.23 becomes:

$$\begin{aligned}\mathcal{L}_{is} = & \frac{1}{2}[\rho_n\omega_n^2 + (\lambda + 2\mu)q^2]|u_l(\vec{q}, \omega_n)|^2 \\ & + \frac{1}{2}[\kappa\omega_n^2 + \rho_sq^2]|\theta(\vec{q}, \omega_n)|^2 \\ & + aq\omega_n u_l(-\vec{q}, -\omega_n)\theta(\vec{q}, \omega_n) \\ & + \frac{1}{2}[\rho_n\omega_n^2 + \mu q^2]|u_t(\vec{q}, \omega_n)|^2\end{aligned}\quad (26)$$

where $u_l(\vec{q}, \omega_n) = iq_i u_i(\vec{q}, \omega_n)/q$ is the longitudinal com-

ponent, $u_t(\vec{q}, \omega_n) = i\epsilon_{ij}q_i u_j(\vec{q}, \omega_n)/q$ are transverse components of the displacement field. Note that Eqn.26 shows that only longitudinal component couples to the superfluid θ mode, while the two transverse components are unaffected by the superfluid mode. This is expected, because the superfluid mode is a longitudinal density mode itself which does not couple to the transverse modes.

From Eqn.26, we can identify the longitudinal-longitudinal phonon correlation function:

$$\langle u_l u_l \rangle = \frac{\kappa\omega_n^2 + \rho_sq^2}{(\kappa\omega_n^2 + \rho_sq^2)(\rho_n\omega_n^2 + (\lambda + 2\mu)q^2) + a^2q^2\omega_n^2} \quad (27)$$

The $\langle \theta\theta \rangle$ and $\langle u_l\theta \rangle$ correlation functions can be similarly written down. By doing the analytical continuation $i\omega_n \rightarrow \omega + i\delta$, we can identify the two poles of all the correlation functions at $\omega_{\pm}^2 = v_{\pm}^2 q^2$ where the two velocities v_{\pm} is given by:

$$v_{\pm}^2 = [\kappa(\lambda + 2\mu) + \rho_s\rho_n + a^2 \pm \sqrt{(\kappa(\lambda + 2\mu) + \rho_s\rho_n + a^2)^2 - 4\kappa\rho_s\rho_n(\lambda + 2\mu)}]/2\kappa\rho_n \quad (28)$$

If setting $a = 0$, then v_{\pm}^2 reduces to the longitudinal phonon velocity $v_{lp}^2 = (\lambda + 2\mu)/\rho_n$ and the superfluid velocity $v_s^2 = \rho_s/\kappa$ respectively. Of course, the transverse phonon velocity $v_{tp}^2 = \mu/\rho_n$ is untouched. For notation simplicity, in the following, we just use v_p for v_{lp} . Inside the SS, due to the very small superfluid density ρ_s , it is expected that $v_p > v_s$. In fact, in isotropic solid He^4 , it was measured that $v_{lp} \sim 450 - 500 m/s$, $v_t \sim 230 \sim 320 m/s$ and $v_s \sim 366 m/s$ near the melting curve²⁰. It is easy to show that $v_+ > v_p > v_s > v_-$ and $v_+^2 + v_-^2 > v_p^2 + v_s^2$, but $v_+v_- = v_p v_s$, so $v_+ + v_- > v_p + v_s$ (see Fig.1). The size of the coupling constant a was estimated to be ~ 0.1 from the slope of the melting curve^{14,33}. So v_+ (v_-) are about 10% above (below) v_p (v_s).

The two longitudinal modes in the SS can be understood from an intuitive picture: inside the NS, it was argued in⁴¹ that there must be a diffusion mode of vacancies in the NS. Inside the SS, the vacancies condense and lead to the extra superfluid mode. So the diffusion mode in the NS is replaced by the SF mode in the SS.

B. *hcp* crystal

Usual single *hcp* crystal samples may also contain dislocations, grain boundaries. Here we ignore these line and plane defects and assume that there are only vacancies whose condensation leads to the superfluid density wave inside the supersolid discussed in sect.V.

For a uni-axial crystal such as an *hcp* lattice, the action

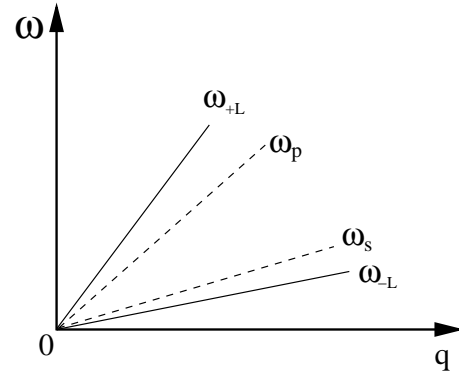


FIG. 6: The elementary low energy excitations inside a supersolid. The coupling between the phonon mode $\omega_p = v_p q$ (the upper dashed line) and the superfluid mode $\omega_s = v_s q$ (the lower dashed line) leads to the two new "supersolidon" modes $\omega_{\pm} = v_{\pm} q$ (solid lines) in the SS. These two new supersolid modes should be detected by in-elastic neutron scatterings.

is:

$$\begin{aligned}
\mathcal{L}_{hcp} = & \frac{1}{2}[\rho_n(\partial_\tau u_\alpha)^2 + K_{11}(u_{xx}^2 + u_{yy}^2) + 2K_{12}u_{xx}u_{yy} \\
& + K_{33}u_{zz}^2 + 2K_{13}(u_{xx} + u_{yy})u_{zz} \\
& + 2(K_{11} - K_{12})u_{xy}^2 + K_{44}(u_{yz}^2 + u_{xz}^2)] \\
& + \frac{1}{2}[\kappa(\partial_\tau \theta)^2 + \rho_z^s(\partial_z \theta)^2 + \rho_\perp^s((\partial_x \theta)^2 + (\partial_y \theta)^2)] \\
& + [a_z \partial_z u_z + a_\perp(\partial_x u_x + \partial_y u_y)]i\partial_\tau \theta \quad (29)
\end{aligned}$$

If \vec{q} is along \hat{z} direction, namely $q_z \neq 0, q_x = q_y = 0$, then Eqn.29 simplifies to:

$$\begin{aligned}
\mathcal{L}_{hcp}^z = & \frac{1}{2}[\rho_n \omega_n^2 + K_{33}q_z^2]|u_z(q_z, \omega_n)|^2 \\
& + \frac{1}{2}[\kappa \omega_n^2 + \rho_z^s q_z^2]|\theta(q_z, \omega_n)|^2 \\
& - ia_z q_z \omega_n u_z(-q_z, -\omega_n) \theta(q_z, \omega_n) \\
& + \frac{1}{2}[\rho_n \omega_n^2 + K_{44}q_z^2/4]|u_t(q_z, \omega_n)|^2 \quad (30)
\end{aligned}$$

where $|u_t(q_z, \omega_n)|^2 = |u_x(q_z, \omega_n)|^2 + |u_y(q_z, \omega_n)|^2$ stand for the two transverse modes with the velocity $v_t^2 = K_{44}/4\rho_n$. The superfluid mode only couples to the longitudinal u_z mode, while the two transverse modes u_x, u_y are decoupled. Eqn.30 is identical to Eqn.26 after the replacement $u_z \rightarrow u_l, K_{33} \rightarrow \lambda + 2\mu, a_z \rightarrow a$. It was found that $v_{lp} \sim 540m/s, v_t \sim 250m/s$ when \vec{q} is along the \hat{z} direction³⁶. Fig.2 follows after these replacements.

Similarly, we can work out the action in the xy plane where $q_z = 0, q_x \neq 0, q_y \neq 0$. Then u_z mode is decoupled, only u_x, u_y modes are coupled to the superfluid mode:

$$\begin{aligned}
\mathcal{L}_{hcp}^{xy} = & \frac{1}{2}[\rho_n(\partial_\tau u_\alpha)^2 + K_{11}(u_{xx}^2 + u_{yy}^2) \\
& + 2K_{12}u_{xx}u_{yy} + 2(K_{11} - K_{12})u_{xy}^2] \\
& + \frac{1}{2}[\kappa(\partial_\tau \theta)^2 + \rho_\perp^s(\partial_\alpha \theta)^2] \\
& + a_\perp \partial_\alpha u_\alpha i\partial_\tau \theta \\
& + \frac{1}{2}[\rho_n(\partial_\tau u_z)^2 + K_{44}/4(\partial_\alpha u_z)^2] \quad (31)
\end{aligned}$$

where $\alpha, \beta = x, y$. By comparing Eqn.31 with Eqn.26, we can see that $K_{11} \rightarrow \lambda + 2\mu, K_{12} \rightarrow \lambda$, so all the discussions in the isotropic case can be used here after the replacements. Fig.2 follows after these replacements. Namely, only the longitudinal component in the xy plane is coupled to the θ mode, while the transverse mode in the xy plane with velocity $v_{txy}^2 = (K_{11} - K_{12})/2\rho_n$ is decoupled. Obviously the transverse mode along \hat{z} direction u_z mode with the velocity $v_{tz}^2 = K_{44}/4\rho_n$ is also decoupled. Note that the two transverse modes have different velocities. It was found that $v_{lp} \sim 455m/s, v_{tz} \sim 255m/s, v_{txy} \sim 225m/s$ when \vec{q} is along the xy plane³⁶.

Along any general direction \vec{q} , strictly speaking, one can not even define longitudinal and transverse modes, so the general action Eqn.29 should be used³⁷. Despite the much involved 4×4 matrix diagonalization in u_x, u_y, u_z, θ ,

we expect the qualitative physics is still described by Fig.2.

In principle, inelastic neutron scattering experiments or acoustic attenuation experiments can be used to detect the predicted the low energy excitation spectra in the SS shown in Fig.2.

VIII. TOPOLOGICAL ELEMENTARY EXCITATIONS IN SS: VORTEX LOOPS AND VORTEX

In section 3, we studied the low energy excitations shown in the Fig.1 by neglecting the topological vortex loop. Here, we will study how the vortex loop interaction in SS differ from that in the SF. For simplicity, in the following, we only focus on the isotropic case. The formulations can be generalized to the *hcp* case straightforwardly. We can perform a duality transformation on Eqn.23 to the vortex loop representation:

$$\mathcal{L}_v = \frac{1}{2K_\mu}(\epsilon_{\mu\nu\lambda\sigma}\partial_\nu a_{\lambda\sigma} - a\partial_\alpha u_\alpha \delta_{\mu\tau})^2 + i2\pi a_{\mu\nu} j_{\mu\nu}^v \quad (32)$$

where $\mu, \nu, \lambda, \sigma$ stand for space and time, but α, β stand for the space components only, $K_0 = \kappa, K_\alpha = \rho_s$ and $a_{\mu\nu} = -a_{\nu\mu}$ is an anti-symmetric tensor gauge field and $j_{\mu\nu}^v = \frac{1}{2\pi}\epsilon_{\mu\nu\lambda\sigma}\partial_\lambda \partial_\sigma \theta$ is the anti-symmetric tensor vortex loop current due to the topological phase winding in θ .

Eqn.32 has the gauge invariance $a_{\mu\nu} \rightarrow a_{\mu\nu} + \partial_\mu \chi_\nu - \partial_\nu \chi_\mu$ where χ_μ is any 4-component field⁴³. It is the most convenient to choose the Coulomb gauge $\partial_\alpha a_{\alpha\beta} = 0$ to get rid of the longitudinal component, then the transverse component is $a_t = i\epsilon_{\alpha\beta\gamma}q_\alpha a_{\beta\gamma}/q$. It can be shown that $|a_t|^2 = 2|a_{\alpha\beta}|^2$. Then Eqn.32 is simplified to:

$$\begin{aligned}
\mathcal{L}_v = & \frac{1}{2}[\rho_n \omega_n^2 + (\lambda + 2\mu + a^2/\kappa)q^2]|u_l(\vec{q}, \omega_n)|^2 \\
& + \frac{1}{2}(q^2/\kappa + \omega_n^2/\rho_s)|a_t|^2 + \frac{2}{\rho_s}q^2|a_{0\alpha}|^2 \\
& - aq^2/\kappa u_l(-\vec{q}, -\omega_n)a_t(\vec{q}, \omega_n) \\
& + i2\pi j_{0\alpha}^v a_{0\alpha} + i2\pi j_{\alpha\beta}^v a_{\alpha\beta} \quad (33)
\end{aligned}$$

where the transverse phonon mode u_t was omitted, because it stays the same as in the NS as shown in Eqn.26.

It is easy to see that only a_t has the dynamics, while $a_{0\alpha}$ is static. This is expected, because although $a_{\mu\nu}$ has 6 non-vanishing components, only the transverse component a_t has the dynamics which leads to the original gapless superfluid mode $\omega^2 = v_s^2 q^2$. Eqn.33 shows that the coupling is between the longitudinal phonon mode u_l and the transverse gauge mode a_t . The vortex loop density is $j_{0\alpha}^v = \frac{1}{2\pi}\epsilon_{\alpha\beta\gamma}\partial_\beta \partial_\gamma \theta$ and the vortex current is $j_{\alpha\beta}^v = \frac{1}{2\pi}\epsilon_{\alpha\beta\gamma}[\partial_0, \partial_\gamma]\theta$. Integrating out the $a_{0\alpha}$, we get the vortex loop density-density interaction:

$$\pi \rho_s \int_0^\beta d\tau \int dx dy j_{0\alpha}^v(\vec{x}, \tau) \frac{1}{|x - y|} j_{0\alpha}^v(\vec{y}, \tau) \quad (34)$$

Namely, the vortex loop density- density interaction in SS stays as $1/r$ which is the same as that in NS ! Therefore, a single vortex loop energy and the critical transition temperature T_{3dxy} in Fig.1 is solely determined by the superfluid density ρ_s independent of any other parameters in Eqn.26, except that the vortex core of the vortex loop is much larger than that in a superfluid¹⁶. The critical behaviors of the vortex loops close to the 3d XY transition was studied in⁴⁰.

In a cylindrical geometry used in the torsional oscillator experiment, the vortex loops will become straight vortex line alone the rotational axis. In the SF phase, a single vortex costs a lot of energy $E_v^{SF} = \frac{\rho_s^{SF} h^2}{4\pi m^2} \ln \frac{R}{\xi_{SF}}$ where m is the mass of He atom, R is the system size and $\xi_{SF} \sim a$ is the core size of the vortex. This energy determines the critical velocity in SF $v_c^{SF} > 30\text{cm/s}$. Because the long distance behavior of SS is more or less the same as SF, we can estimate its single vortex energy $E_v^{SS} = \frac{\rho_s^{SS} h^2}{4\pi m^2} \ln \frac{R}{\xi_{SS}}$ where ρ_s^{SS} is the *global* superfluid density inside the SS. We expect the core size of a supersolid vortex $\xi_{SS} \sim 1/\Lambda \gg 1/k_r \sim a \sim \xi_{SF}$. So inside the SS vortex core, we should also see the lattice structure of n ³². This is similar to the phenomenon that DW ordered states were detected in the vortex core of high temperature superconductors^{30,31}. In fact, because $\psi(x)$ stands for vacancies or interstitials, we expect that ξ_{SS}

should be of the order of the average spacing between the interstitials or vacancies in the SS. It is interesting to see if neutron or light scattering experiments can test this prediction. Compared to E_v^{SF} , there are two reductions, one is the superfluid density, another is the increase of the vortex core size $\xi_{SS} \gg \xi_{SF}$. These two factors contribute to the very low critical velocity $v_c^{SS} \sim 30\mu\text{m/s}$. Of course, the reduction from the increase of the vortex core is negligible because of the logarithmic dependence.

Integrating out the $a_{\alpha\beta}$, we get the vortex loop current-current interaction:

$$2\pi^2 j_{\alpha\beta}^v(-\vec{q}, -\omega_n) D_{\alpha\beta,\gamma\delta}(\vec{q}, \omega_n) j_{\gamma\delta}^v(\vec{q}, \omega_n) \quad (35)$$

where $D_{\alpha\beta,\gamma\delta}(\vec{q}, \omega_n) = (\delta_{\alpha\gamma}\delta_{\beta\delta} - \delta_{\beta\gamma}\delta_{\alpha\delta} - \frac{q_\beta q_\delta}{q^2}\delta_{\alpha\gamma} - \frac{q_\alpha q_\gamma}{q^2}\delta_{\beta\delta} + \frac{q_\alpha q_\delta}{q^2}\delta_{\alpha\delta} + \frac{q_\beta q_\gamma}{q^2}\delta_{\alpha\delta}) D_t(\vec{q}, \omega_n)$ where $D_t(\vec{q}, \omega_n)$ is the a_t propagator. Defining $\Delta D_t(\vec{q}, \omega_n) = D_t^{SS}(\vec{q}, \omega_n) - D_t^{SF}(\vec{q}, \omega_n)$ as the difference between the a_t propagator in the SS and the SF, then from Eqn.33, we can get:

$$\Delta D_t = \frac{a^2 \rho_s^2 q^4}{\kappa \rho_n (\omega_n^2 + v_+^2 q^2) (\omega_n^2 + v_-^2 q^2) (\omega_n^2 + v_s^2 q^2)} \quad (36)$$

For simplicity, we just give the expression for the equal time

$$\Delta D_t(\vec{x} - \vec{x}', \tau = 0) = \frac{a^2 \rho_s^2}{4\pi^2 \kappa^2 \rho_n^2} \frac{v_+ + v_- + v_s}{(v_+ + v_-)(v_s + v_+)(v_s + v_-) v_+ v_- v_s} \frac{1}{(\vec{x} - \vec{x}')^2} \quad (37)$$

Namely, the vortex current-current interaction in SS is stronger than that in the SF with the same parameters κ, ρ_s !

IX. X-RAY SCATTERING FROM THE SS

Let's look at the prediction of our theory on X-ray scattering from the SS. For a lattice with $j = 1, \dots, n$ basis located at \vec{d}_j , the geometrical structure factor at the reciprocal lattice vector \vec{K} is $S(\vec{K}) = \sum_{j=1}^n f_j(\vec{K}) e^{i\vec{K} \cdot \vec{d}_j}$ where f_j is the atomic structure factor of the basis at \vec{d}_j . The X-ray scattering amplitude $I(\vec{K}) \sim |S(\vec{K})|^2$. Again, we discuss SS-v and SS-i respectively.

A. X-ray scattering from the SS-v

In this case, because the superfluid density wave simply sits on the n lattice, so the X-ray scattering is very similar to that from NS at mean field level. However, as shown

B. X-ray scattering from the SS-i

In this case, as shown in section VI, the superfluid density wave is shifted from n lattice, so the X-ray scattering is different from that from NS even at mean field level. For simplicity, we first take the *sc* lattice to explain the main points, then list the X-ray scattering from all the other lattices classified in section VI.

(a) Simple Cubic lattice. For the SS in the *sc* lattice, as shown in (c2) of the last section, the local superfluid density attains its maximum at the dual lattice points of the *sc* lattice. Then $\vec{d}_1 = 0, \vec{l}_1 = \frac{a}{2}(\vec{i} + \vec{j} + \vec{k}), \vec{K} = \frac{2\pi}{a}(n_1 \vec{i} + n_2 \vec{j} + n_3 \vec{k})$, then taking the ratio of the geometric structure factor of SS over that of the NS $S_{SS}(\vec{K})/S_{NS} = 1 + f(-1)^{n_1+n_2+n_3}$ where $f \sim \rho_s^{max} \sim a^2$. It is $1 + f$ for even \vec{K} and $1 - f$ for odd \vec{K} .

(b) Triangular lattice. $\vec{d}_1 = 0, \vec{l}_1 = \frac{1}{3}(\vec{a}_1 + \vec{a}_2), \vec{l}_2 =$

$\frac{2}{3}(\vec{a}_1 + \vec{a}_2)$, $\vec{K} = n_1\vec{b}_1 + n_2\vec{b}_2$, then taking the ratio of the geometric structure factor of SS over that of the NS $S_{SS}(\vec{K})/S_{NS} = 1 + 2f \cos \frac{2\pi}{3}(n_1 + n_2)$. This result could be relevant to possible 2d excitonic superfluid in electron-hole bilayer system to be briefly mentioned in section X.

(c) *hcp* lattice. *hcp* lattice is not a Bravais lattice. In NS, $\vec{d}_1 = 0$, $\vec{d}_2 = \frac{1}{3}(\vec{a}_1 + \vec{a}_2) + \vec{a}_3/2$, $\vec{K} = n_1\vec{b}_1 + n_2\vec{b}_2 + n_3\vec{b}_3$, then $S_{NS}(\vec{K}) = 1 + e^{i2\pi(\frac{n_1+n_2}{3} + \frac{n_3}{2})}$. In the SS, there are 2 more additional basis at $\vec{l}_1 = \frac{2}{3}(\vec{a}_1 + \vec{a}_2) + \vec{a}_3/4$, $\vec{l}_2 = 3\vec{a}_3/4$, then $S_{SS}(\vec{K}) = S_{NS}(\vec{K}) + fe^{i2\pi(\frac{2(n_1+n_2)}{3} + \frac{n_3}{4})} + fe^{i\frac{3\pi}{2}n_3} = S_{NS}(\vec{K}) + fe^{-i\frac{\pi}{2}n_3}S_{NS}^*(\vec{K})$.

(d) *bcc* lattice. We think *bcc* lattice as a *sc* lattice plus a basis, $\vec{d}_1 = 0$, $\vec{d}_2 = \frac{a}{2}(\vec{i} + \vec{j} + \vec{k})$, $\vec{K} = \frac{2\pi}{a}(n_1\vec{i} + n_2\vec{j} + n_3\vec{k})$, Then $S_{NS}(\vec{K}) = 1 + (-1)^{n_1+n_2+n_3}$ which is 2 for even \vec{K} and 0 for odd \vec{K} . In the SS, there are 3 more additional basis at $\vec{l}_1 = \frac{a}{2}(\vec{i} + \vec{j})$, $\vec{l}_2 = \frac{a}{2}(\vec{i} + \vec{k})$, $\vec{l}_3 = \frac{a}{2}(\vec{j} + \vec{k})$, then $S_{SS}(\vec{K}) = S_{NS}(\vec{K}) + f[(-1)^{n_1+n_2} + (-1)^{n_1+n_3} + (-1)^{n_2+n_3}]$.

(e) *fcc* lattice. We think *fcc* lattice as a *sc* lattice plus 4 basis located at $\vec{d}_1 = 0$, $\vec{d}_2 = \frac{a}{2}(\vec{i} + \vec{j})$, $\vec{d}_3 = \frac{a}{2}(\vec{i} + \vec{k})$, $\vec{d}_4 = \frac{a}{2}(\vec{j} + \vec{k})$, $\vec{K} = \frac{2\pi}{a}(n_1\vec{i} + n_2\vec{j} + n_3\vec{k})$, then $S_{NS}(\vec{K}) = 1 + [(-1)^{n_1+n_2} + (-1)^{n_1+n_3} + (-1)^{n_2+n_3}]$. In the SS, there is one more additional basis located at $\vec{l}_1 = \frac{a}{2}(\vec{i} + \vec{j} + \vec{k})$, then $S_{SS}(\vec{K}) = S_{NS}(\vec{K}) + f(-1)^{n_1+n_2+n_3}$. It is easy to see that in *bcc* and *fcc* lattices, we need simply exchange d vectors for the NS and the l vectors for SFDW.

We conclude that the elastic X-ray scattering intensity from the SS-i has an additional modulation over that of the NS. The modulation amplitude is proportional to the maxima of the superfluid density $\rho_s^{max} \sim a^2$ which is the same as the NCRI observed in the PSU's torsional oscillator experiments.

C. Debye-Waller factor in the X-ray scattering from the SS-v and SS-i

It is known that due to zero-point quantum motion in any NS at very low temperature, the X-ray scattering

amplitude $I(\vec{G})$ will be diminished by a Debye-Waller (DW) factor $\sim e^{-\frac{1}{3}G^2\langle u_\alpha^2 \rangle}$ where u_α is the lattice phonon modes in Eqn.23. In Eqn.23, if the coupling between the \vec{u} and θ were absent, then the DW factor in the SS would be the same as that in the NS. By taking the ratio $I_{SS}(\vec{G})/I_{NS}(\vec{G})$ at a given reciprocal lattice vector \vec{G} , then this DW factor drops out. However, due to this coupling, the $\langle u_\alpha^2 \rangle$ in SS is different than that in NS, so the DW factor will *not* drop out in the ratio. In this subsection, we will calculate this ratio and see how to take care of this factor when comparing with the X-ray scattering data.

As identified below Eqn.18, the density order parameter at the reciprocal lattice vector \vec{G} is $\rho_{\vec{G}}(\vec{x}, \tau) = e^{i\vec{G} \cdot \vec{u}(\vec{x}, \tau)}$, then $\langle \rho_{\vec{G}}(\vec{x}, \tau) \rangle = e^{-\frac{1}{2}G_i G_j \langle u_i u_j \rangle}$. The Debye-Waller factor:

$$I(\vec{G}) = |\langle \rho_{\vec{G}}(\vec{x}, \tau) \rangle|^2 = e^{-G_i G_j \langle u_i(\vec{x}, \tau) u_j(\vec{x}, \tau) \rangle} \quad (38)$$

where the phonon-phonon correlation function is:

$$\langle u_i u_j \rangle = \langle u_l u_l \rangle \hat{q}_i \hat{q}_j + \langle u_t u_t \rangle (\delta_{ij} - \hat{q}_i \hat{q}_j) \quad (39)$$

$$\text{where } \hat{q}_i \hat{q}_j = \frac{q_i q_j}{q^2} \cdot \cdot$$

Then substituting Eqn.39 into Eqn.38 leads to:

$$\alpha(\vec{G}) = I_{SS}(\vec{G})/I_{NS}(\vec{G}) = e^{-\frac{1}{3}G^2[\langle u_l^2(\vec{x}, \tau) \rangle_{SS} - \langle u_l^2(\vec{x}, \tau) \rangle_{NS}]} \quad (40)$$

where the transverse mode drops out, because it stays the same in the SS and in the NS.

Defining $(\Delta u^2)_l(\vec{q}, i\omega_n) = \langle |u_l(\vec{q}, i\omega_n)|^2 \rangle_{SS} - \langle |u_l(\vec{q}, i\omega_n)|^2 \rangle_{NS}$, $(\Delta u^2)_l(\vec{q}) = \sum_{i\omega_n} (\Delta u^2)_l(\vec{q}, i\omega_n)$ and $(\Delta u^2)_l = \langle u_l^2(\vec{x}, \tau) \rangle_{SS} - \langle u_l^2(\vec{x}, \tau) \rangle_{NS} = \int \frac{d^3q}{(2\pi)^d} \frac{1}{\beta} \sum_{i\omega_n} (\Delta u^2)_l(\vec{q}, i\omega_n) = \int \frac{d^3q}{(2\pi)^d} (\Delta u^2)_l(\vec{q})$, it is easy to see:

$$(\Delta u^2)_l = \int \frac{d^3q}{(2\pi)^3} \frac{1}{\beta} \sum_{i\omega_n} \frac{-a^2 q^2 \omega_n^2}{[(\kappa\omega_n^2 + \rho_s q^2)(\rho_n \omega_n^2 + (\lambda + 2\mu)q^2) + a^2 q^2 \omega_n^2][\rho_n \omega_n^2 + (\lambda + 2\mu)q^2]} \quad (41)$$

Obviously, $(\Delta u^2)_l < 0$, namely, the longitudinal vibration amplitude in SS is *smaller* than that in NS. The $\alpha(\vec{G})(T = 0) = e^{-\frac{1}{3}G^2(\Delta u)_l} 1$. This is expected, because the SS state is the ground state at $T < T_{SS}$, so the longitudinal vibration amplitude should be reduced compared to the corresponding NS with the same parameters ρ_n, λ, μ .

After evaluating the frequency summation in Eqn.41, we get:

$$(\Delta u^2)_l(T) = \int \frac{d^3q}{(2\pi)^3} \frac{1}{\rho_n} \left[\frac{\coth \beta v_+ q/2}{2v_+ q} - \frac{\coth \beta v_p q/2}{2v_p q} - \left(\frac{v_s^2 - v_-^2}{v_+^2 - v_-^2} \right) \left(\frac{\coth \beta v_+ q/2}{2v_+ q} - \frac{\coth \beta v_- q/2}{2v_- q} \right) \right] \quad (42)$$

At $T = 0$, the above equation simplifies to:

$$\begin{aligned}
 (\Delta u^2)_l(T=0) &= \int \frac{d^3q}{(2\pi)^3} \frac{1}{\rho_n} \left[\frac{1}{2v_+q} - \frac{1}{2v_-q} \right. \\
 &\quad \left. - \left(\frac{v_s^2 - v_-^2}{v_+^2 - v_-^2} \right) \left(\frac{1}{2v_+q} - \frac{1}{2v_-q} \right) \right] \\
 &= -\frac{(v_+ + v_- - v_p - v_s)}{(v_+ + v_-)v_p} \frac{\Lambda^2}{8\pi^2\rho_n} \\
 &= -\frac{a^2}{\kappa\rho_n} \frac{1}{(v_+ + v_- + v_p + v_s)(v_+ + v_-)v_p} \frac{\Lambda^2}{8\pi^2\rho_n} < 0 \quad (43)
 \end{aligned}$$

where $\Lambda \sim 1/a$ is the ultra-violet cutoff and we have used the fact $v_+ + v_- > v_p + v_s$.

By subtracting Eqn.43 from Eqn.42, we get

$$\begin{aligned}
 &(\Delta u^2)_l(T) - (\Delta u^2)_l(T=0) = \\
 &\frac{(v_+ - v_p)(v_+ + v_p) - (v_s - v_-)(v_+ + v_-)}{(v_+ + v_-)v_+v_-v_p^2} \frac{(k_B T)^2}{12\rho_n} > 0 \quad (44)
 \end{aligned}$$

Namely, the difference in the ratio will *decrease* as T^2 as the temperature increases. Of course, when T approaches T_{SS} from below, the difference vanishes, the $\alpha(\vec{G})$ will approach 1 from above, the SS turns into a NS.

D. Density-density correlations

The density-density correlation function in the SS is:

$$\langle \rho_{\vec{G}}(\vec{x}, t) \rho_{\vec{G}}^*(\vec{x}', t') \rangle = e^{-\frac{1}{2}G_i G_j \langle (u_i(\vec{x}, t) - u_i(\vec{x}', t'))(u_j(\vec{x}, t) - u_j(\vec{x}', t')) \rangle} \quad (45)$$

where t is the real time.

For simplicity, we only evaluate the equal-time correlator $\langle \rho_{\vec{G}}(\vec{x}, t) \rho_{\vec{G}}^*(\vec{x}', t) \rangle = \langle \rho_{\vec{G}}(\vec{x}, \tau) \rho_{\vec{G}}^*(\vec{x}', \tau) \rangle$ where τ is the imaginary time. It is instructive to compare the density order in SS with that in a NS by looking at the ratio of the density correlation function in the SS over the NS:

$$\alpha_\rho(\vec{x} - \vec{x}') = \langle \rho_{\vec{G}} \rho_{\vec{G}}^* \rangle_{SS} / \langle \rho_{\vec{G}} \rho_{\vec{G}}^* \rangle_{NS} = e^{-\frac{1}{6}G^2 \Delta D_\rho(\vec{x} - \vec{x}')} \quad (46)$$

It is easy to find that

$$\Delta D_\rho(\vec{x} - \vec{x}') = \int \frac{d^3q}{(2\pi)^3} (2 - e^{i\vec{q} \cdot (\vec{x} - \vec{x}')} - e^{-i\vec{q} \cdot (\vec{x} - \vec{x}')})(\Delta u^2)_l(\vec{q}) \quad (47)$$

where $(\Delta u^2)_l(\vec{q})$ is defined above Eqn.41 and is the integrand in Eqn.42.

At $T = 0$, the above equation can be simplified to

$$\Delta D_\rho(\vec{x} - \vec{x}') = \frac{(v_+ + v_- - v_p - v_s)}{(v_+ + v_-)v_p} \frac{1}{2\pi^2\rho_n} \frac{1}{(\vec{x} - \vec{x}')^2} \quad (48)$$

So we conclude that $\alpha_\rho(\vec{x} - \vec{x}') < 1$, namely, the density order in SS is *weaker* than the NS with the corresponding parameters ρ_n, λ, μ . This is expected because the density order in the SS is weakened by the presence of moving vacancies.

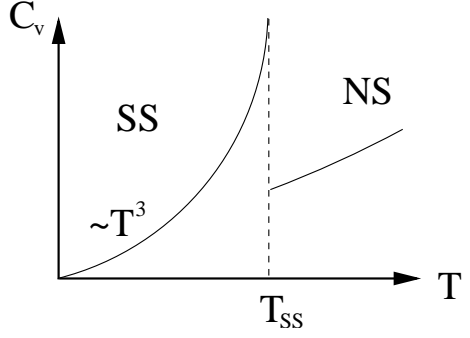


FIG. 7: The specific heat of a supersolid

Unfortunately, so far, the X-ray scattering data is limited to high temperature $T > 0.8K > T_{SS}$ ²⁹. X-ray scattering experiments on lower temperature $T < T_{SS}$ are being performed to test these predictions.

X. SPECIFIC HEAT IN THE SS

It is well known that at low T , the specific heat in the NS is $C^{NS} = C_{lp}^{NS} + C_{tp}^{NS} + C_{van}$ where $C_{lp}^{NS} = \frac{2\pi^2}{15} k_B (\frac{k_B T}{\hbar v_{lp}})^3$ is from the longitudinal phonon mode and $C_{tp}^{NS} = 2 \times \frac{2\pi^2}{15} k_B (\frac{k_B T}{\hbar v_{tp}})^3$ is from the two transverse phonon modes, while C_{van} is from the vacancy contribution. C_{van} was calculated in³⁹ by assuming 3 different kinds of models for the vacancies. So far, there is no consistency between the calculated C_{van} and the experimentally measured one^{15,39}. The specific heat in the SF $C_v^{SF} = \frac{2\pi^2}{15} k_B (\frac{k_B T}{\hbar v_s})^3$ is due to the SF mode θ . In this subsection, we focus on the specific heat inside the SS. From Eqn.26, we can find the specific heat in the SS:

$$C_v^{SS} = \frac{2\pi^2}{15} k_B (\frac{k_B T}{\hbar v_+})^3 + \frac{2\pi^2}{15} k_B (\frac{k_B T}{\hbar v_-})^3 + C^{tp} \quad (49)$$

where C^{tp} stands for the contributions from the transverse phonons which are the same as those in the NS (Fig.7).

It was argued in¹⁶, the critical regime of finite temperature NS to SS transition in Fig.1 is much narrower than the that of SF to the NL transition, so there should be a jump in the specific heat at $T = T_{SS}$ (Fig.7). Eqn.49 shows that at $T < T_{SS}$, the specific heat still takes $\sim T^3$ behavior and is dominated by the ω_- mode in Fig.6.

From Eqn.49, it is easy to evaluate the entropy inside the SS:

$$S_{SS}(T_{SS}) = \frac{2\pi^2}{45} k_B (\frac{k_B T_{SS}}{\hbar})^3 (\frac{1}{v_+^3} + \frac{1}{v_-^3}) + S^{tp} \quad (50)$$

where S^{tp} is the entropy due to the 2 transverse modes.

The *excess* entropy due to the vacancy condensation

is:

$$\Delta S = \int_0^{T_{SS}} dT C_{van}/T = \frac{2\pi^2}{45} k_B \left(\frac{k_B T_{SS}}{\hbar} \right)^3 \left(\frac{1}{v_+^3} + \frac{1}{v_-^3} - \frac{1}{v_{lp}^3} \right) \quad (51)$$

Obviously, $\Delta S > 0$ is due to the lower branch $v_- < v_{lp}$. At $a = 0$, the above equation reduces to $\Delta S = \frac{2\pi^2}{45} k_B \left(\frac{k_B T_{SS}}{\hbar v_s} \right)^3$ which is simply the vacancy condensation into SF. Using the molar volume $v_0 \sim 20 \text{ cm}^3/\text{mole}$ of solid ^4He and $T_{ss} \sim 100 \text{ mK}$, we can estimate the ΔS per mole is $\sim 10^{-5} \text{ R}$ where R is the gas constant. This estimate is 3 orders magnitude smaller than that in⁴⁷ where the SS state was taken simply as the boson condensation of non-interacting vacancies. Our estimate is indeed consistent with recent experiment on specific heat⁴⁶. The linear $\sim T$ behaviour found in heat capacity experiment can only be due to disorder or ^3He impurities.

XI. DISCUSSIONS ON PSU'S AND OTHER EXPERIMENTS AND APPLICATIONS IN OTHER SYSTEMS

In subsections 1 to 3, we make very speculative comments on some relevant experiments from the phenomenological GL theory. For an alternative view from numerical calculations, see⁴⁵. Then in subsections 4 to 6, we make connections to other related systems.

1. The effects of He3 impurities

Although the NS to SS transition is in the same universality class as the NL to SF one, it may have quite different off-critical behaviours due to the SFDW structure in the SS state. We can estimate the critical regime of the NS to SS transition from the Ginsburg Criterion $t_G^{-1} \sim (\xi_{SS}^3 \Delta C)^2$ where ΔC is the specific jump in the mean field theory. Because of the cubic dependence on ξ_{SS} , large ξ_{SS} leads to extremely narrow critical regime, the 3D XY critical behavior is essentially irrelevant, instead mean field Gaussian theory should apply. Assuming ^3He impurities diffusion process is slow, we can use this fact to address two experimentally observable effects of the He3 impurities. Both have been indeed observed experimentally. (1) slightly below T_{SS} , the vortex pairs are in the dilute vortex limit where the unbinding transition temperature T_{SS} is determined by the pinning due to impurities instead of by the logarithmic interactions between the vortices which is proportional to the superfluid stiffness. So the He3 impurities effectively pin the vortices and raise the unbinding critical temperature T_{SS} . Taking the He3 impurity concentration $x \sim 0.3 \text{ ppM}$, the average distance d_{imp} between the He3 impurities is $d_{imp} \sim 450 \text{ \AA} \sim 120a$, the average distance between a vortex pair is $R_p > \xi_{SS} \gg a$, we expect $R_p \sim d_{imp}$, the vortex pair is indeed effectively pinned by the He3 impurities at such a tiny concentration. On the other hand, He3 impurities will certainly decrease the superfluid density in both the ψ_1 and ψ_2 sector just like He3 impurities decreases superfluid density in the ^4He superfluid. Note

that in ^4He superfluid, slightly below T_{SF} , the vortex pairs are in the dense vortex limit where the unbinding transition temperature T_{SF} is determined by the logarithmic interactions between the vortices which is proportional to the superfluid stiffness. So in ^4He SF, He3 impurities hurt superfluid density which, in turn, lead to the reduction in T_{SF} . In short, the He3 impurities play a dual role in the SS phase, on the one hand, they raise the unbinding critical temperature T_{SS} of the vortices, on the other hand, they decrease the superfluid density in both ψ_1 and ψ_2 sector. Indeed, in the PSU's experiments, in an isotropically stressed sample, as the concentration of He3 impurities decreases, the T_{SS} drops considerably, but the NCRI rises. In contrast, in both 3d superfluid ^4He and 2d superfluid ^4He films, He3 impurities hurt both the superfluid stiffness and T_c . So the role played by He3 impurities in the PSU experiments is similar to the disorder played in fractional quantum Hall effects: the disorder is needed to even have a fractional quantized Hall plateau, but the quantum Hall liquid ground state is completely due to the strong Coulomb interaction among electrons and exists even in the absence of disorder. However, too much disorder will also destroy the fractionally quantized Hall plateau just like too much He3 impurities will also destroy the superfluid density. (2) In principle, in clean system, the specific heat measurement should show the λ peak as the NL to SF transition does. Because the 3d XY specific heat exponent $\alpha = -0.012 < 0$, from the Harris criterion, we conclude that weak disorder will not change the universality class of the 3d XY model describing the SS to the NS transition, so will not destroy the λ peak. However, due to very narrow critical regime, it will be very difficult to observe the λ peak. So the 3D XY critical behavior of the NS-SS transition is essentially irrelevant in the PSU experiments, instead mean field Gaussian theory should apply where there should be a specific heat jump at $T = T_{SS}$. The mean field jump maybe smeared by the presence of He3 impurities. Indeed, recent very refined specific heat measurements indeed found a broadened specific heat peak around $\sim 100 \text{ mK}$ when $x \sim 0.3 - 3 \text{ ppM}$. We conclude that the broadened specific heat peak around $\sim 100 \text{ mK}$ in the presence of He3 impurities is closely related to the opposite trend of the dependence of T_{SS} and the superfluid density on the concentration of He3 impurities.

2. Other torsional oscillator, mass flow and acoustic wave experiments

Recently, a Cornell group lead by Reppy found that the NCRI signal detected by the PSU group can be eliminated through a crystal annealing process¹⁸. There are two possible explanations for this observation (1) This corresponds to $|g_v| > |g_{vc}|$ where the Fig.2 holds. There could be vacancies in the thermodynamic stable ground state whose condensation leads to the SS-v in the Fig.2. The annealing process simply push the He3 impurities to the boundary, so reduces the supersolid transition temperature T_{SS} as discussed in 1. (2) This corresponds to $|g_v| < |g_{vc}|$ where the Fig.1 holds. A state with vacancies

is just a metastable state, then the supersolid state is just a metastable state. Annealing not only gets rid of the He_3 impurities, but also vacancies, so reduce or eliminate the metastable SS-v state. Even so, a SS-v metastable state maybe interesting and deserves the investigations done in this paper. The PSU group did the same annealing process which, in fact, last much longer than Cornell's group did, so should result even better single crystal with even better quality, but the supersolid signal (NCRI effect) stays more or less the same. One of the main points of the manuscript is that the X-ray scattering experiment on SS-v, if can be performed at low enough temperature, can be very helpful to resolve the debate.

Beamish's group¹⁹ found that there is no detectable mass flow driven by pressure difference in solid Helium in Vycor at temperature as low as 48 mK and pressure 60 bar. It is important to resolve the puzzle that why the SFDW behaves like a superfluid in the torsional oscillator experiment, but does not response sensitively to a pressure difference.

By acoustic attenuation and heat wave experiments³⁸, Goodkind discovered that the solid 4He displays a phase transition below 200 mK only if it is strained or in the presence of He_3 impurities also in the concentration range of $\sim ppM$. This observation is consistent with the PSU's torsional oscillator experiments. The mechanism proposed in 1 may also lead to a natural explanation of Goodkind's observation.

3. Analogy with Type-I and Type-II superconductors

Finally, it may be instructive to make some analogy of Fig.1 and Fig.2 at $T < T_{SF}$ to Type-I and type-II superconductors with the pressure p playing the role of the magnetic field H : Fig.1 is similar to Type-I superconductor with SF identified as the Messiner state, the NS as the normal state, the critical pressure p_c identified as the critical magnetic field H_c . Fig.2 is similar to Type II superconductor with SF identified as the Messiner state, the SS as the mixed vortex lattice state which also breaks both translational order and the global $U(1)$ symmetry, the NS as the normal state, the lower and upper critical pressures p_{c1} and p_{c2} identified as the lower and upper critical magnetic fields H_{c1} and H_{c2} . In superconductors, it is the $\kappa = \lambda/\xi$ to determine Type I and Type II and if the vortex lattice is a stable intermediate state or not as the magnetic field is increased. In Helium 4, it is the sign and strength of the coupling constant g in Eqn.3 to determine the Fig.1 and Fig.2 and if the SS is a stable intermediate state or not as the pressure is increased. *So the pressure p and the coupling g in the formation of SS-v play the role of the magnetic field H and κ in the formation of the mixed state of superconductors.* Note that in superconductors, H and κ are two independent parameters, in 4He , p and g are also two independent parameters.

4. Absence of supersolid in solid hydrogen

The solid (para)-hydrogen H_2 also takes the hcp lattice. As explained in the introduction, so far, no NCRI was discovered in H_2 solid. Although H_2 are even

lighter than 4He , it has deeper attractive potential, so smaller de Boer quantum number. Bulk H_2 solidifies at $T < T_c \sim 14K$ even at zero pressure, this fact preempts the possible observation of the speculated SF state. At $T = 0$, due to the absence of the adjacent SF state, the quantum fluctuations are not strong enough to produce vacancies or interstitials in the H_2 solid, so the solid is a commensurate solid. Therefore, no SS is possible. As shown in section V, approaching from the SF side, the vacancies or interstitials originate from the condensation of rotons, so in a continuous system, a SS state can not exist without the existence of an adjacent SF state in the first place. We conclude there is no supersolid in H_2 . One potential avenue to prevent $p - H_2$ from being solidified to low enough temperature such that the superfluid behavior can be observed is by depositing H_2 on external substrates which can disrupt the deep H_2 potential. It was suggested in⁵⁴ that a judicious choice of substrate may be able to lead to an occurrence of hydrogen lattice supersolid.

XII. CONCLUSIONS

The PSU's experiments renewed the interests in the 4He system which already had fantastic properties. In this paper, we constructed a two component QGL theory to map out the 4He phase diagram, analyze carefully the conditions for the existence of the supersolid and study all the phases and phase transitions in a unified view. The only new parameters introduced in the GL theory in this paper is the coupling g and v between the n sector (or normal solid part) and the ψ sector (or the superfluid part) in Eqn.3. We investigated the SS state from both the SF and the NS side and found completely consistent description of the properties of the SS state. Starting from the SF side with increasing the pressure, we developed the theory basing on the two facts (1) there is a roton minimum in the superfluid state (2) the instability to solid formation is driven by the gap diminishing at the roton minimum. By increasing the pressure from the superfluid side, there are two possible scenarios (1) the SF to the C-NS transition in Fig.1 was described by the QGL action Eqn.11 first derived in this paper (2) the SF to the SS transition in Fig.2 is a simultaneous combination of the SFDW transition in the ψ sector driven by the roton condensation at $k_0 = k_r$ and the NS transition in the n sector driven by the divergence in the structure function $k_0 = k_n = k_r$. The superfluid becomes a SS at lower temperature and a NS at higher temperature (Fig.2). Then we also approached the SS state from the NS side. Depending on the sign and strength of the coupling g between the solid and superfluid, we also found two possible scenarios: (1) If $|g|$ is sufficiently small (Fig.4), then the resulting solid at $T = 0, p_{c1} < p < p_{c2}$ is a commensurate normal solid (C-NS). The SS state does not exist as a ground state. However, it may still exist as a metastable state. The QGL action to describe

this SF to NS transition in Fig.1 was developed in Sec.II. (2) If $|g|$ is sufficiently large (Fig.4), the resulting solid at $T = 0, p_{c1} < p < p_{c2}$ is an incommensurate solid with zero point quantum fluctuations generated vacancies if it is negative and interstitials if it is positive (Fig.4). The condensation of the vacancies or interstitials lead to the formation of the SS-v and SS-i respectively. The SS state has lower energy than the NS state at $T = 0$. The T_{SS-v} (T_{SS-i}) is an effective measure of the strength of the interaction in the SS-v (SS-i) supersolid. There is no particle-hole symmetry relating T_{SS-v} to T_{SS-i} . Our results showed that SS-v is more likely than SS-i. For completeness reason, we discuss both SS-v and SS-i on the same footing although SS-i is less likely to be relevant to 4He system. Many physical consequences came out of this single parameter g . Our results on supersolid should be independent of many microscopic details and universal.

Just like the SF is a uniform two-component phase consisting of superfluid and normal component at any finite temperature, the SS state is a *uniform* two-component phase consisting of a superfluid density wave (SFDW) and a normal solid component even at zero temperature. The SFDW in the SS-v coincides with the underlying normal solid. While the SFDW in the SS-i state is just a dual lattice to the underlying normal solid. This important fact leads to the key prediction in this paper: the X-ray scattering intensity from the SS-v is similar to that of NS at mean field level, while the X-ray scattering intensity from the SS-i ought to have an additional modulation over that of the NS. The modulation amplitude is proportional to the Non-Classical Rotational-Inertial (NCRI) observed in the torsional oscillator experiments. These prediction are amenable to ongoing X-ray scattering experiments on 4He at very low temperature. However, the X-ray scatterings from SS-v and SS-i will be modified by the Debye-Waller factor calculated in sec. VIII. The NS-v (NS-i) to SS-v (SS-i) transition is described by a 3d XY model with much narrower critical regime (Fig.4). The fact that the critical regime of the NS to SS transition is much narrower than the NL to SF transition leads to the two experimentally observable effects of He3 impurities. (1) The He3 impurities decrease the superfluid density, but increase the critical temperature transition T_{SS} from the SS to the NS transition. (2) The He3 impurities may smear specific heat jump at $T = T_{SS}$ into a broad peak. Indeed, an excessive specific heat anomaly around $\sim 100\text{ mK}$ has been detected in very recent refined experiments in the samples with $x \sim 0.3 - 3\text{ ppm}$ at PSU. By studying all the phases in a unified framework, we conclude there is no SS in hydrogen. We also made comments on several other experiments.

We also studied the zero temperature quantum phase transition from the SS to the NS driven by the pressure near the upper critical pressure $p = p_{c1}$ in Fig.1. We found that the coupling to the quantum fluctuation of the underlying lattice is irrelevant, so the transition stays

the same universality class as the superfluid to Mott insulator transition in a 3 dimensional rigid optical lattice. The finite temperature transition from the SS to the NS in Fig.1 was studies previously in¹⁴ and in³³ in different contexts. It was found that the coupling to classical elastic degree of freedoms will not change the universality class of the 3D XY transition. However, we found that the coupling to quantum lattice phonons is very important inside the SS and leads to two "supersolidon" modes $\omega_{\pm} = v_{\pm}q$ (one upper branch and one lower branch) shown in Fig.2. The transverse modes in the SS stays the same as those in the NS. Detecting the two supersolidon modes, especially, the lower branch ω_- mode by neutron scattering or acoustic wave attention experiments is a smoking gun experiment to prove or disprove the existence of the SS in helium 4He . The ω_- is estimated to be even 10% lower than the sound speed in the superfluid. Then we calculated the experimental signature of the two supersolidon modes. We found that the longitudinal vibration in the SS is smaller than that in the NS (with the same corresponding solid parameters), so the Debye-Waller factor at a given reciprocal lattice vector is larger than that in the NS. The density-density correlation function in the SS is weaker than that in the NS. By going to the dual vortex loop representation, we found the vortex loop density-density interaction in SS stays the same as that in the SF (with the same corresponding superfluid parameters), so the vortex loop energy and the corresponding SS to NS transition temperature is solely determined by the superfluid density and independent of any other parameters. The vortex current-current interaction is stronger than that in the SF. The specific heat in the SS is still given by the sum from the transverse phonons and the two supersolidon modes and still shows $\sim T^3$ behaviors. The supersolidon part is dominated by the lower branch. The NCRI is only weakly anisotropic in the SS phase for *hcp* lattice. In principle, all these predictions can be tested by experimental techniques such as X-ray scattering, neutron scattering, acoustic wave attenuations and heat capacity.

If the supersolid state is responsible for the NCRI observed in PSU's experiments remains controversial. The GL theory developed in this paper put the competing orders of superfluid and solid in the unified framework. It can be used to address many questions raised in PSU's experiments and other experiments and to make predictions to be tested by future experiments. It can also be applied to study possible supersolid state in other continuous bosonic and electronic systems such as fermionic supersolid, BLQH and electron-hole bilayer system. We suggest that even supersolid may not be realized in 4He system, it has its own intrinsic, scientific interests and may be realized in other continuous bosonic and fermionic systems.

Acknowledgement

I thank P. W. Anderson, M. Chan, T. Clark, Milton Cole, B. Halperin, Jason Ho, J. K. Jain, T. Leggett, T. Lubensky, Mike Ma, G. D. Mahan, S. Sachdev and F. C.

Zhang for helpful discussions, A. T. Dorsey for pointing out Ref.²³ to me. The research at KITP was supported by the NSF grant No. PHY99-07949. I also thank the hospitality of Y. Chen, Z. Wang and F. C. Zhang during my visit at Hong Kong University, Yu Lu during my visit at Institute for Theoretical Physics in Beijing, China.

APPENDIX A: DISCUSSIONS ON A TIGHT-BINDING TOY SUPERSOLID GROUND STATE WAVEFUNCTION

The Ginzburg-Landau theory constructed in the main text is based on order parameters and symmetries. It should hold irrespective many microscopic details such as what is the mechanism responsible for the formation of the supersolid. Despite there are many microscopic calculations for 4He , constructing a microscopic theory for supersolid is very difficult. In this appendix, I will discuss a well known toy SS wavefunction and clarify a few concepts related to *global* phase-number uncertainty relation and the role of vacancies or interstitials in the formation of SS. We also clarify the physical meaning of the order parameters n in Eqn.1 and ψ in Eqn. 2. However, because the toy wavefunction may miss some important physics in bulk 4He systems. For example, due to the very peculiar potential well in the solid 4He which has a local shallow maximum at the lattice site, the tight binding model is very crude. The extended Bloch states described in section VI works much better. Furthermore, Eqn.A1 is built on a rigid lattice, as explained in sec.X, it does not include phonon excitations, so the discussion is intuitive and instructive.

Inside the SF state, because of the strong hard core and long-range correlations between the bare 4He atoms, the order parameter ψ in Eqn. 2 is related to, but should not be taken as the bare 4He atom annihilation operator, namely, $n(\vec{x}) \neq \psi^\dagger(\vec{x})\psi(\vec{x})$. Inside the NS phase, its physical meaning need some explanations. In this section, we discuss the physical meanings of ψ and n in Eqns.1, 2, 3 inside the SS state from a toy wavefunction of the SS state.

The toy wavefunction of a supersolid takes the BCS like form

$$|SS\rangle = \prod_{i=1}^N (u + vb_i^\dagger)|0\rangle \quad (\text{A1})$$

where $u \neq 0$ and $|u|^2 + |v|^2 = 1$. If setting $u = 0$, the state reduces to a commensurate solid without any vacancies $|CS\rangle = \prod_{i=1}^N b_i^\dagger|0\rangle$. The commensurate solid (CS) is an exact eigenstate of the boson number operator $N_b = \sum_{i=1}^N n_i$ with the eigenvalue $N_b = N$, so has no chance to become phase ordered. Adding a superfluid component to the CS leads to the SS in Eqn.A1. If setting $v = 0$, then the state reduces to the vacuum state $|0\rangle$.

If setting $u = \cos \frac{\theta}{2}, v = \sin \frac{\theta}{2} e^{i\phi}$, then Eqn.A1 be-

comes:

$$|SS, \phi\rangle = \prod_{i=1}^N (\cos \frac{\theta}{2} + \sin \frac{\theta}{2} e^{i\phi} b_i^\dagger)|0\rangle \quad (\text{A2})$$

where $\theta \neq \pi$.

By construction, the state has the translational order with the average boson density $\langle n_i \rangle = |v|^2 = \sin^2 \theta/2$, so the average vacancy density is $|u|^2 = \cos^2 \theta/2$. It is easy to see that $|SS\rangle$ also has the ODLRO with $\langle b_i \rangle = u^* v = \frac{1}{2} \sin \theta e^{i\phi}$, so $|SS\rangle$ is indeed a supersolid state. The angle θ controls the magnitude, while the phase ϕ controls the phase of the condensation. Defining $b_{k=0} = \frac{1}{\sqrt{N}} \sum_{i=1}^N b_i$ which satisfy the boson commutation relation $[b_0, b_0^\dagger] = 1$, the boson operator at zero momentum is $n_0 = b_{k=0}^\dagger b_{k=0}$, the total number of bosons at the zero momentum state is $N_0 = \langle SS|n_0|SS\rangle = \frac{N}{4} \sin^2 \theta = N_b \cos^2 \theta/2 < N_b = N \sin^2 \theta/2 < N$. At integer filling $n = 1$, the non-interacting BEC state $|SF\rangle = \frac{1}{\sqrt{N!}} (b_{k=0}^\dagger)^N |0\rangle$, then $N_0 = \langle SF|n_0|SF\rangle = N_b = N$. Obviously, this non-interacting BEC state is not included in the family in the Eqn.A1.

A supersolid state $|SS, N_b\rangle$ with N_b bosons is given by:

$$|SS, N_b\rangle = \int_0^{2\pi} \frac{d\phi}{2\pi} e^{-iN_b\phi} |SS, \phi\rangle \quad (\text{A3})$$

where the total boson number N_b and the global phase ϕ are two Hermitian conjugate variables satisfying the commutation relation: $[N_b, \phi] = i\hbar$. It leads to the uncertainty relation $\Delta N_b \Delta \phi \geq 1$.

It is easy to see $\langle N_b \rangle = N|v|^2 = N \sin^2 \theta/2, \Delta N_b = \sqrt{\langle N_b^2 \rangle - \langle N_b \rangle^2} = \sqrt{N|uv|} = \sqrt{N \frac{1}{2} |\sin \theta|}, \Delta N_b / \langle N_b \rangle = \frac{1}{\sqrt{N}} |u/v| = \frac{1}{\sqrt{N}} |\cot \theta/2|$. If $\theta \neq \pi$, the absolute boson number fluctuation $\Delta N_b \sim \sqrt{N}$ is quite large, so $\Delta \theta$ could be quite small, so one can get a phase ordered state. On the other hand, the relative boson number fluctuation $\Delta N_b / \langle N_b \rangle \sim \frac{1}{\sqrt{N}}$ is quite small, so one can still measure the average boson number accurately. The first quantization form of the Eqn.A3 can be derived by the same method used in²¹.

Because in the SS state, there is a global phase ordering in ϕ , so its conjugate variable is the total number of particles N_b as shown in Eqn.A3. The local tunneling or exchanging processes stressed in⁴ may not cause the total number fluctuations, therefore may not cause the global phase ordering leading to the supersolid phase. The discussions in this appendix is at most instructive. It is known that state Eqn.A1 may not describe the ground state of the solid 4He Hamiltonian well, but what it implies is that if the vacancies in an incommensurate solid could lead to the formation of a supersolid. In this indeed happens, in the GL theory constructed for SS-v in the main text, the bosons are represented by $n(x)$, while the vacancies are represented by ψ . A toy wavefunction for SS-i is not written down so far, because the interstitials are moving between lattice sites, so there is no

tight binding limit. The interstitial case is described by the extended Bloch state in Section VI-B. In the SS-i, the bosons are represented by $n(x)$, while the interstitials are represented by ψ .

APPENDIX B: COMPARISONS WITH SUPERSOLID ON LATTICES

Supersolids on lattice models were studied in⁴⁴. The GL theory, especially the coupling between n sector and ψ sector in⁴⁴ are different than those in Eqn.1, Eqn. 2, Eqn.3 in bulk 4He system constructed in this paper. In⁴⁴, due to the lack of ψ components in non-zero reciprocal lattice vectors \vec{G} , the first non-trivial coupling is the quartic term $\sum'_{\vec{G}} v_{\vec{G}} |n_{\vec{G}}|^2 |\psi|^2$. Indeed, if we only consider the ψ mode near $\vec{k} = 0$, then the v term in Eqn.3 reduces to this term. In Eqn.3, we also have the most important additional cubic term $g\delta n(\vec{x})|\psi|^2$ in Eqn.3. This crucial difference make the two GL theories completely differently.

The extended boson Hubbard model (EBHM) with various kinds of interactions, on all kinds of lattices and at different filling factors is described by the following Hamiltonian³⁵:

$$H = -t \sum_{\langle ij \rangle} (b_i^\dagger b_j + h.c.) - \mu \sum_i n_i + \frac{U}{2} \sum_i n_i(n_i - 1) + V_1 \sum_{\langle ij \rangle} n_i n_j + V_2 \sum_{\langle\langle ik \rangle\rangle} n_i n_k + \dots \quad (B1)$$

where $n_i = b_i^\dagger b_i$ is the boson density, t is the nearest neighbor hopping amplitude. U, V_1, V_2 are onsite, nearest neighbor (nn) and next nearest neighbor (nnn) interactions respectively, the \dots may include further neighbor interactions and possible ring-exchange interactions. A supersolid in Eqn.B1 is defined as the simultaneous orderings of ferromagnet in the XY component (namely, $\langle b_i \rangle \neq 0$) and CDW in the Z component. In⁵⁴, we studied all the possible phases and phase transitions in the EBHM in bipartite lattices such as a honeycomb and square lattice near half filling. We show that there are two consecutive transitions at zero temperature *driven by the chemical potential*: in the Ising limit, a Commensurate-Charge Density Wave (CDW) at half filling to a narrow window of CDW supersolid, then to an Incommensurate-CDW ; in the easy-plane limit, a Commensurate-Valence Bond Solid (VBS) at half filling to a narrow window of VBS supersolid, then to an Incommensurate-VBS. The first transition is second order in the same universality class as the Mott to insulator transition , therefore has the exact critical exponents $z = 2, \nu = 1/2, \eta = 0$ with logarithmic corrections, while the second one is first order. Liu and Fisher⁴⁴ also studied the C-CDW to the CDW-SS transition and concluded that $z = 1$ in contrast to $z = 2$ achieved in⁵⁴. We found that the phase diagram in the Ising limit is similar to the

reentrant "superfluid" in a narrow region of coverages in the second layer of 4He adsorbed on graphite detected by Crowell and Reppy's torsional oscillator experiment in 1993⁵⁶. It is still not clear if the extended boson Hubbard model can describe the experimental situation well. But the results suggest that 4He lattice supersolid may have been already observed in 1993 which was 11 years earlier than the PSU's experiments on bulk 4He . Indeed, the data in the torsional oscillator experiment in⁵⁶ do not show the characteristic form for a 2d 4He superfluid film, instead it resembles that in⁷ characteristic of a supersolid in terms of the gradual onset temperature of the NCRI, the unusual temperature dependence of T_{SS} on the coverage. Of course, both experiments may due to phase separations instead of the SS phase. very recently, the author studied various kinds od supersolids in frustrated lattices such as triangular and kagome lattices⁵⁵.

It is known that a lattice system is different than a continuous system in many ways. We can compare Eqns.1, 2,3 in the continuum with the Eqn.B1 on the lattice. (1) Eqn 1 stands for a spontaneously formed lattice with phonon excitations. While Eqn.B1 is a fixed external lattice with no such phonon excitations. (2) Eqn. 2 shows the bosons are in extended Bloch waves, because the bosons are so dilute $\sim 1\%$, so their mutual interaction u is not important, except when two bosons are very close to each other. While Eqn.B1 shows the bosons are in the tight binding limit. The bosons are in a very dense limit $\sim 50\%$, so the boson-boson interactions are dominant (3) Eqn.3 shows that the lattice-boson (or lattice phonon-boson) interactions are dominant and drives the the NS to SS transition. while there is simply no such lattice phonon-boson interaction in Eqn.B1. So the reentrant lattice SS discussed in^{44,54,55} is different from the bulk 4He SS state discussed in this paper, although both kinds of supersolids share many interesting common properties. In both cases, the SF to SS transition is driven by the closing of the gap of the roton minimum. On the lattice, the manifold of the roton minimum consists of discrete points due to the lattice symmetry, so the transition could be 1st or second order. However, in 4He , as shown in sections III and IV, the manifold of the roton minimum is a continuous surface, so the transition must be first order. In the former, there is a periodic substrate or spacer potential which breaks translational symmetries at the very beginning. The filling factor is controlled by an external chemical potential. There are particle-hole symmetry for excitations at integer filling factors which ensure the number of particles is equal to that of vacancies and at half filling factors which ensure adding interstitials is equivalent to adding vacancies^{54,55}. While in the latter, the lattice results from a spontaneous translational symmetry breaking driven by the pressure as shown in the Fig.2, if there are vacancies or interstitials in the ground state has to be self-determined by ground state energy minimization. There is usually no particle-hole symmetry for excitations. Due to this absence of symmetry, the number of vacancies is usually not equal

to that of interstitials. So the theory developed in this paper on bulk 4He is different from the lattice theory developed in^{44,54}. As shown in the appendix and in^{54,55}, one common fact of both supersolids is that both are due to vacancies or interstitials. Lattice supersolids can also be described by doping the adjacent CDW either by vacancies or interstitials, so are classified as two types $SS - v$ and $SS - i$. In the hard-core limit, $SS - v$ and $SS - i$ are simply related by P-H transformation. However, as shown in section VI, in Helium-4 supersolid, there is no particle-hole symmetry relating T_{SS-v} to T_{SS-i} (Fig.3) ! *So the coupling constant g in Helium 4 plays a similar role as the chemical potential μ in the lattice models, the gap $\Delta(p)$ in the NS-PH which tunes the distance from the NS-PH to the SF plays a similar role as the gap in the CDW which tunes the distance from the CDW to the superfluid .* It was shown in⁵⁵, the lattice supersolids existing at commensurate 1/2 filling factors in frustrated lattices such as triangular lattice is just the coexistence of SS-v and SS-i. Combined with the results in⁵⁴, we conclude that 4He supersolid can exist both in bulk and on substrate, while although H_2 supersolid may not exist in the bulk, but it may exist on wisely chosen substrates. Lattice supersolid could also be realized in optical lattices in ultra-cold atomic experiments^{6,59}. However, in both continuum and on lattices, SS states could be unstable against phase separations. For example, the vacancies or interstitials in the in-commensurate solid can simply move to the boundary of the sample instead of boson condensation, namely, it will turn into a commensurate solid. This case is included in the C-NS case in the paper anyway. Due to its negative compressibility, the instability of lattice SS against phase separation was demonstrated in some lattice models in^{60,61}.

APPENDIX C: POSSIBLE EXCITONIC SUPERSOLIDS IN FERMIONIC SYSTEMS

Although 2d bilayer quantum Hall system (BLQH) is a fermionic system, it was argued there exists excitonic superfluid (ESF) state in the pseudo-spin channel⁴⁸. In real space, one exciton is an electron in one layer paired with a hole in another layer (with respect to the underlying $\nu = 1$ integer quantum Hall state), its size is of the same order of the interlayer distance, so could be viewed as a boson in the pseudo-spin channel. In^{49,50,51}, starting from the ESF state, as the distance increases, we studied the instability due to the collapsing of the magneto-roton minimum at q_0 which leads to the formation of the pseudo-spin density wave (PSDW). We showed that a square lattice is the favorite lattice for the

PSDW. The interlayer distance in BLQH play a similar role as the pressure in 4He . Unlike in 4He where the lattice constant is *self-determined* by the pressure, the lattice constant a of the resulting PSDW is completely fixed by the filling factor which is *independent of the distance*, due to the slight mismatch between the lattice constant a and the instability point $1/q_0$, the resulting PSDW is likely to be an *in-commensurate* solid where the number of sites N_s may not be the same as the number of excitons N even at $T = 0$. As the distance increases further $d_{c1} < d < d_{c2}$, the PSDW lattice constant is still *locked* at the same value a . Assuming zero-point quantum fluctuations favor vacancies over interstitials, we take $N < N_s$, so there are vacancies n_0 even at $T = 0$ in both top and bottom layers. As argued in⁴⁹, the correlated hopping of vacancies in the active and passive layers in the PSDW state leads to very large and temperature dependent drag consistent with the experimental data. However an excitonic supersolid (ESS) is very unlikely in BLQH. In symmetric electron-hole bilayer systems⁵², it was shown in⁴² that it is quite possible that there may a narrow window of ESS where both order parameters are non-vanishing $\langle \psi \rangle \neq 0, \langle n_{\vec{G}} \rangle \neq 0$ intervening between the ESF and two weakly coupled Wigner crystal.

In fermionic systems, it is easy to see the coexistence of CDW and Superconductivity (SC), so " fermionic supersolid " phases are common. For instance, a quasi- two-dimensional system NbSe₂ has a transition to an incommensurate CDW phase at some high temperature T_{CDW} and then a transition to a phase with coexisting CDW and SC order at a lower temperature T_{SC} . The CDW is a pairing in particle-hole channel at $2k_F$, its order parameter is $\psi_{CDW} = \langle c_{\sigma}^{\dagger}(\vec{k})c_{\sigma}(\vec{k} + \vec{Q}) \rangle$ where \vec{Q} is the ordering wave vector of the CDW. The SC is a pairing in particle-particle channel also across the Fermi surface. Its order parameter is $\psi_{SC} = \langle c_{\uparrow}^{\dagger}(\vec{k})c_{\downarrow}^{\dagger}(-\vec{k}) \rangle$. Both order parameters are composite order parameters. Different parts of Fermi surface can do the two jobs separately (see, for example,⁵³). In contrast to the bosonic SS where there is a density operator n and a complex order parameter ψ , both order parameters ψ_{CDW} and ψ_{SC} are complex order parameters. We can see that although the formation of a supersolid in a bosonic system has completely different mechanism as shown in this paper, from symmetric point of view, the QGL theories constructed in this paper could also be used to describe the interplay between the two complex order parameters, the properties of the " fermionic supersolid " (FSS) and the transition from the FSS to the CDW. However, the fermionic excitations near the nodes maybe also be important and need to be taken into account⁵³.

¹ C. N. Yang, Rev. Mod. Phys. **34**, 694 (1962).

² A. Andreev and I. Lifshitz, Sov. Phys. JETP **29**, 1107

(1969).

³ G. V. Chester, Phys. Rev. A **2**, 256 (1970).

⁴ A. J. Leggett, Phys. Rev. Lett. **25**, 1543 (1970).

⁵ W. M. Saslow , Phys. Rev. Lett. 36, 1151?1154 (1976).

⁶ For review of NCRI in atomic gases, see Franco Dalfovo, Stefano Giorgini, Lev P. Pitaevskii and Sandro Stringari, Rev. Mod. Phys. 71, 463?512 (1999); Anthony J. Leggett , Rev. Mod. Phys. 73, 307?356 (2001).

⁷ E. Kim and M. H. W. Chan, Nature 427, 225 - 227 (15 Jan 2004).

⁸ E. Kim and M. H. W. Chan, Science 24 September 2004; 305: 1941-1944.

⁹ A. Clark and M. Chan, J. Low Temp. Phys. **138**, 853 (2005).

¹⁰ E. Kim, M. H. W. Chan, Phys. Rev. Lett. **97**, 115302 (2006).

¹¹ A. C. Clark, X. Lin, M. H. W. Chan, cond-mat/0610240.

¹² D. M. Ceperley, B. Bernu, Phys. Rev. Lett. **93**, 155303 (2004); N. Prokof'ev, B. Svistunov, Phys. Rev. Lett. **94**, 155302 (2005); D. E. Galli, M. Rossi, L. Reatto, Phys. Rev. B 71, 140506(R) (2005); Evgeni Burovski, Evgeni Kozik, Anatoly Kuklov, Nikolay Prokof'ev, Boris Svistunov, Phys. Rev. Lett., vol. 94, p. 165301 (2005). M. Boninsegni, A. B. Kuklov, L. Pollet, N. V. Prokof'ev, B. V. Svistunov, and M. Troyer, Phys. Rev. Lett. **97**, 080401 (2006).

¹³ W. M. Saslow, Phys. Rev. B **71**, 092502 (2005); N. Kumar, cond-mat/0507553; G. Baskaran, cond-mat/0505160; Xi Dai, Michael Ma, Fu-Chun Zhang, Phys. Rev. B 72, 132504 (2005).

¹⁴ A. T. Dorsey, P. M. Goldbart, J. Toner, Phys. Rev. Lett. **96**, 055301 (2006).

¹⁵ P. W. Anderson, W. F. Brinkman, David A. Huse, Science 18 Nov. 2005; 310: 1164-1166.

¹⁶ Jinwu Ye, Phys. Rev. Lett. 97, 125302 (2006).

¹⁷ Jinwu Ye, Europhysics Letters, 82 (2008) 16001.

¹⁸ Ann Sophie C. Rittner, John D. Reppy, Phys. Rev. Lett. 97, 165301 (2006).

¹⁹ James Day, T. Herman and John Beamish, Phys. Rev. Lett., vol 95, 035301 (2005).

²⁰ I. A. Todoshchenko, H. Alles, J. Bueno, H. J. Junes, A. Ya. Parshin, and V. Tsepelin, Phys. Rev. Lett. 97, 165302 (2006)

²¹ Gun Sang Jeon and Jinwu Ye, Phys. Rev. B 71, 035348 (2005) .

²² T. Schneider and C. P. Enz, Phys. Rev. Lett. 27, 1186 (1971); Yves Pomeau and Sergio Rica , Phys. Rev. Lett. 72, 2426 (1994).

²³ P. Nozieres, J. Low. Temp. Phys. 137, 45 (2004).

²⁴ Guenter Ahlers , Phys. Rev. A 3, 696C716 (1971); Dennis S. Greywall and Guenter Ahlers , Phys. Rev. A 7, 2145C2162 (1973).

²⁵ For discussions on Classical Lifshitz Point (CLP) and their applications in nematic to smectic-A and -C transitions in liquid crystal, see the book by P. M. Chaikin and T. C. Lubensky, Principles of Condensed Matter Physics, Cambridge university press,1995.

²⁶ S. A. Brazovskii, JETP 41, 85 (1975).

²⁷ Feynman originally conceived the roton as drifting vortex loop. But this point of view is very controversial. If taking this view, then the roton condensation can be considered as vortex loop condensation.

²⁸ In 2 + 1 dimensional Bilayer quantum Hall systems, the magnetoroton dispersion relation is $\omega^2 \sim q^2(a - bq + cq^2)$ due to long-range Coulomb interaction. See⁴⁹.

²⁹ B. A. Fraass, P. R. Granfors, and R. O. Simmons, Phys. Rev. B 39, 124C131 (1989); C. A. Burns and E. D. Isaacs, Phys. Rev. B 55, 5767C5771 (1997).

³⁰ J. E. Hoffman *et al.* Science 295, 466 (2002).

³¹ S. R. White and D. J. Scalapino, Phys. Rev. Lett, 80, 1272 (1998).

³² The core energy is always much smaller than the superflow energy even for large size of vortex core.

³³ M. A. De Moura, T. C. Lubensky, Y. Imry, and A. Aharony, Phys. Rev. B 13, 2176 (1976); D. Bergman and B. Halperin, Phys. Rev. B 13, 2145 (1976).

³⁴ W. Saslow, Phys. Rev. B **15**, 173 (1977); M. Liu, Phys. Rev. B **18**, 1165 (1978); M. Bijlsma, H. Stoof, Phys. Rev. B **56**, 14631 (1997).

³⁵ Fisher M. P. A., Weichman P. B., Grinstein G. and Fisher D. S. Phys. Rev. B 40, 546 (1989).

³⁶ R. H. Crepeau *et al.* Phys Rev A 3, 1162 (1971); D. S. Greywall, Phys Rev A 3, 2106 (1971).

³⁷ In a general direction which is neither along \hat{z} nor in xy plane, exactly perpendicular or parallel conditions are not met. However, one can still use the notions of quasi-transverse and quasi-longitudinal modes as done in the Fig.10 in the first reference in³⁶. One can project the direction onto the z-axis and xy-plane, the elastic constants in the velocity expressions are just some effective average of the 5 different elastic constants.

³⁸ John M. Goodkind, Phys. Rev. Lett. 89, 095301 (2002); G. Lengua and J. M. Goodkind, J. Low Temp. Phys. 79, 251 (1990)

³⁹ C.A. Burns and J.M. Goodkind, J. Low Temp. Phys. 95, 695 (1994).

⁴⁰ G. A. Williams, Phys. Rev. Lett. 82, 1201 (1999)

⁴¹ P. C. Martin, O. Parodi, and P. S. Pershan, Phys. Rev. A 6, 2401 (1972)

⁴² The $d = 2$ analog of Eqn.19 and Eqn.23 where the 2d lattice can be taken as a triangular lattice with only 2 elastic constants may describe the excitations in a 2d excitonic SS in electron-hole bilayer system. Jinwu Ye, arXiv:0712.0437.

⁴³ In fact, if setting $a = 0$, Eqn.32 can be written in a Lorentz invariant form: $\mathcal{L}_v = \frac{1}{3K_\mu} H_{\mu\nu\lambda}^2 + i2\pi a_{\mu\nu} j_{\mu\nu}^v$ where $H_{\mu\nu\lambda} = \partial_\mu a_{\nu\lambda} + \partial_\nu a_{\lambda\mu} + \partial_\lambda a_{\mu\nu}$ is gauge invariant under the gauge transformation $a_{\mu\nu} \rightarrow a_{\mu\nu} + \partial_\mu \chi_\nu - \partial_\nu \chi_\mu$. However, this neat form is not of practical use in the presence of the a coupling term in Eqn.32.

⁴⁴ K. S. Liu and M. E. Fisher, Jour of Low Temp. Phys. 10, 655, (1973).

⁴⁵ Prokof'ev, cond-mat/0612499.

⁴⁶ X. Lin, A. C. Clark and M. H. W. Chan, Nature, 06228, 2007.

⁴⁷ A. V. Balatsky, M. J. Graf, Z. Nussinov and S. A. Trugman, Phys. Rev. B 75, 094201 (2007).

⁴⁸ For a review, see S. M. Girvin and A. H. Macdonald, in *Perspectives in Quantum Hall effects*, edited by S. Das Sarma and A. Pinczuk (Wiley, New York, 1997).

⁴⁹ Jinwu Ye and Longhua Jiang, Phys. Rev. Lett. 98, 236802 (2007).

⁵⁰ Jinwu Ye, Phys. Rev. Lett 97, 236803 (2006).

⁵¹ Jinwu Ye, Annals of Physics, 323 (2008), 580-630.

⁵² L. V. Butov, C. W. Lai, A. L. Ivanov, A. C. Gossard, D. S. Chemla, L. V. Butov, A. C. Gossard, D. S. Chemla, Nature 418, 751 - 754 (15 Aug 2002). D. Snoke, S. Denev, Y. Liu, L. Pfeiffer, K. West, Nature 418, 754 - 757 (15 Aug 2002). David Snoke, Nature 443, 403 - 404 (28 Sep 2006). C. W. Lai, J. Zoch, A. C. Gossard, and D. S. Chemla, Science 23

January 2004 303: 503-506. U. Sivan, P. M. Solomon, and H. Shtrikman, Phys. Rev. Lett. 68, 1196C1199 (1992). S. De Palo¹*, F. Rapisarda², and Gaetano Senatore¹, Phys. Rev. Lett. 88, 206401 (2002).

⁵³ A. H. Castro Neto, Phys. Rev. Lett, 86, 4382 (2001).

⁵⁴ Jinwu Ye, Nucl. Phys.B 805 (3) 418-440 (2008).

⁵⁵ Jinwu Ye, cond-mat/0612009.

⁵⁶ P. A. Crowell and J. D. Reppy, Phys. Rev. Lett. 70, 3291C3294 (1993); Phys. Rev. B 53, 2701C2718 (1996).

⁵⁷ P.W. Anderson; Science 235, 1196(1987).

⁵⁸ H. Wiechert and K. Kortmann, Phys. Rev. B 70, 125410 (2004).

⁵⁹ M. Greiner, O. Mandel, T. Esslinger, T. W. Hansch, T. Bloch, Nature 415, 39-44 (2002).

⁶⁰ G. C. Batrounil *et al*, Phys. Rev. Lett. 74, 2527 (1995); *ibid*, 84, 1599 (2000).

⁶¹ Pinaki Sengupta, *et al*, Phys. Rev. Lett. 94, 207202 (2005).

⁶² Ganpathy Murthy, Daniel Arovas, Assa Auerbach, Phys. Rev. B 55, 3104 (1997).